https://doi.org/10.5194/egusphere-2024-1601
Preprint. Discussion started: 5 June 2024

Synoptic background of the Adriatic Sea high-frequency sea-level extremes

Krešimir Ruić[1], Jadranka Šepić[1], Marin Vojković[1]

[1]Faculty od science, University of Split, Split, 21000, Croatia

Correspondence to: Krešimir Ruić (kruic@pmfst.hr)

Abstract. Large oscillations in sea-level can pose significant threats to coastal communities and endanger infrastructure. The large sea-level variations are driven by different physical processes that occur on various spatial and temporal scales. This study focuses on the high-frequency component (periods shorter than 2 hours) of sea-level oscillations, particularly those induced by atmospheric processes. Episodes of extreme high-frequency sea level oscillations were identified at six tide gauge stations in the Adriatic Sea using the peak-over-threshold method. The length of time series was ~17 years. Characteristic synoptic situations preceding the Extremes were extracted using the k-medoid clustering method applied on the ERA5 reanalysis data. Analyses were conducted on the following ERA5 fields: mean sea-level pressure (MSLP), temperature at 850 hPa, and geopotential at 500 hPa. The structural similarity index measure (SSIM) was used as the distance metric. The data were divided into a training set (from the start of measurements to the beginning of 2018) and a testing set (from the beginning of 2018 to the end of 2020). For each station, k-medoid method was applied for selection of both 2 and 3 characteristic clusters. Two types of synoptic situations leading to extreme high-frequency sea level oscillations were extracted for all stations: "bad-weather" situation which favours both storm surges and intense high-frequency sea level oscillations, and "good-weather" situation which favours only intense high-frequency sea-level oscillations. The two situations mostly differ in surface fields, with the "bad-weather" situation characterised by larger MSLP gradients over the Adriatic and stronger surface winds. At higher levels, situations are more similar, and mostly described by inflow of warm air from the south-west and strong westerly to south-westerly jet stream. Inclusion of the third clusters led to refinement of one of two characteristic situations at all stations aside for Bakar and Rovinj where it led to a new "bora (strong north-easterly wind) -favourable" situation. The extracted clusters were used to label all days of the testing period, with particular attention given to days in which episodes of extreme high-frequency sea-level oscillations occurred. The potential of using k-medoid method for future prediction of these high-frequency, atmospherically induced sea-level oscillations is discussed.

1 Introduction

Sea-level variability manifests itself on time scales from seconds to millennia and on spatial scales from a centimetre to the global scale (Pugh and Woodworth, 2014). In this paper, we focus on short-period sea-level variability (also referred to as a high-frequency variability), which occurs on temporal scales of a few minutes to 2-6 hours and on spatial scales of a few to thousands of kilometres, and which includes long ocean waves, edge waves and seiches. Long

https://doi.org/10.5194/egusphere-2024-1601
Preprint. Discussion started: 5 June 2024

ocean waves are progressive waves with a large wavelength and a small amplitude compared to the ocean depth, propagating at a speed c given by $c = \sqrt{gh}$, where g is the gravity acceleration, and h is the ocean depth (Pugh and Woodworth, 2014). Long ocean waves include waves with long periods (tidal periods and longer), that are affected by the Coriolis force (e.g. Kelvin waves; Pugh and Woodworth, 2014), as well as waves with shorter periods for which gravity is the only restoring force, such as tsunamis (Pugh and Woodworth, 2014). Edge waves are travelling waves that propagate along the coast at a speed that depends on the inclination of the sea floor (Ursell, 1952). Seiches are standing oscillations in an enclosed basin (such as a lake) or in a locally isolated part of a basin (such as inlet, bay, or channel) which have periods from minutes up to a day (Rabinovich, 2009). All listed sea-level oscillations can be triggered by tsunami-generating processes such as (i) earthquakes, (ii) subaerial or submarine landslides; (iii) volcanic eruptions, and (iv) meteorite impacts (Fine et al., 2003; Levin and Nosov, 2009), but also by atmospheric and oceanic processes, such as wind disturbances, propagating air pressure disturbances and incoming long ocean waves (Monserrat et al., 2006; Bechle and Wu, 2014). In this paper, only atmospherically induced sea-level oscillations are considered.

The strongest atmospherically triggered short-period sea-level oscillations are often referred to as meteorological tsunamis (or meteotsunamis; Monserrat et al., 2006). The definition of a meteotsunami is not a unique one. Monserrat et al. (2006) state that "meteotsunamis are tsunami-like waves that are induced by atmospheric processes rather than by seismic sources. However, such definition, if given without an amplitude/strength condition, leads to a vast number of meteotsunamis, as atmospheric processes continuously generate long ocean waves of variable amplitude, but rarely of a destructive one. Nowadays, most authors set a threshold for the identification of a meteotsunami. Sometimes this value is set to a specific height (e.g., 100 cm for the Adriatic Sea, Orlić, 2015; Šepić and Orlić, 2024), sometimes it is a station-dependent value (e.g., Rabinovich and Monserrat, 1996) and sometimes it is a combination of a fixed and station-dependent value (Dusek et al., 2019)

The atmospheric processes which lead to development of short period sea-level oscillations are dominantly wind (Wilson, 1972) and atmospheric pressure disturbances (Monserrat et al., 2006). A connection between atmospheric pressure disturbances and short period sea-level oscillations was suggested at the beginning of the 20th century when Honda et al. (1908) who studied seiches of Japanese harbours noted that "…these undulations (i.e., seiches) seem to be associated with unstable distribution of atmospheric pressure, in which case a sudden local change of pressure is liable to take place". In 1929, Proudman published a seminal theoretical paper (Proudman, 1929) in which he proposed a resonance mechanism acting between propagating atmospheric pressure disturbances and long ocean waves in a channel. The process, which was later named "The Proudman resonance" by Orlić (1980), is now widely accepted as a main atmospheric mechanism controlling generation of intense short-period long ocean waves. In the Mediterranean, a simultaneity of short-period atmospheric and ocean oscillations was noticed as early as the 1930s (e.g., for the Balearic Islands; Fontserè, 1934). Further seminal studies include (but are not limited to), chronologically, papers by Ewing et al. (1954), Orlić (1980), and Hibiya and Kajiura (1982). Ewing et al. (1954) investigated the Chicago tsunami-like waves of June 26, 1954, in which 7 people lost their lives, and associated the waves with a propagating pressure jump. Orlić (1980) suggested that the Proudman resonance

https://doi.org/10.5194/egusphere-2024-1601
Preprint. Discussion started: 5 June 2024

was responsible for the large tsunami waves in Vela Luka on June 21, 1978, and Hibiya and Kajiura (1982) showed, through numerical modelling, that a three-stage resonance process (Proudman resonance, shelf resonance and harbour resonance) is required to explain the destructive seiche/meteosunami which occurred in Nagasaki Bay in 1979. Modern understanding of meteotsunamis was developed largely on these initial studies.

Intense short-period sea-level oscillations, such as meteotsunamis, are often observed during calm summer weather and low background sea-level (termed as "good-weather" meteotsunamis; Rabinovich, 2020). Therefore, strong meteotsunamis often come as a surprise and thus can pose a great danger to beach visitors and coastal population. However, destructive short-periods sea level oscillations can also appear jointly with a storm surge (termed as "bad-weather meteotsunamis; Rabinovich, 2020) - in this case, two types of oscillations combine to form hazardous sea-level heights. Storm surges are generated by tropical and extratropical cyclones through the inverse barometric and wind piling effect (Pugh and Woodworth, 2014). Over mid-latitudes, atmospheric instabilities associated with the cyclone's warm and cold fronts often lead to steep, short-period atmospheric pressure changes and related strong winds which can trigger long ocean waves. Some examples of extreme events where maximum sea-level was caused by the joint acting of storm surge and high frequency sea-level oscillations include: Storm Gudrun in the Baltic Sea (Suursaar et al., 2006), Storm Gloria in the western Mediterranean (Pérez-Gómez et al., 2021), Typhoons Lionrock and Jebi on the coasts of Japan (Heidarzadeh and Rabinovich, 2021), Typhoon Maysak in Korea and the Sea of Japan (Medvedev et al., 2022), Typhoon Songda and related extratropical cyclones in British Columbia and Washington State (Rabinovich et al., 2023).

Although many individual events of extreme short period sea-level oscillations have been analysed in detail – through theoretical studies, atmospheric and ocean data analysis, and numerical modelling (see Rabinovich, 2020 for an extensive list of research on the strongest known meteotsunamis) - statistical analyses of multiple events are not nearly as numerous. The main challenge lies in the lack of sufficiently long series of high-quality sea-level data, measured with time steps shorter than 10 minutes. National operators only started to measure sea-level data with shorter time steps at the end of the 20th and beginning of the 21st century, but these data are usually not high-quality, and thus require extensive post-processing (Zemunik et al., 2021a). Today, there are high-quality databases, albeit mostly of hourly sea-level data (e.g. GESLA – also containing some higher resolution data; Haigh et al., 2022), which allow for a detailed investigation of extremes occurring at periods longer than 2 hours. However, there are very few databases that contain quality-controlled higher resolution data. One of the exceptions is the NOAA database, which contains quality-checked 6-minute sea-level data (https://tidesandcurrents.noaa.gov/). Using the NOAA data, Beckle et al. (2016) and Dusek et al. (2019) performed the first comprehensive statistical analyses of sea-level extremes occurring at periods shorter than 6 hours along the Great Lakes and the USA East Coast, respectively, with both studies revealing that these oscillations can pose a significant risk for the coastal area. Šepić et al. (2015a) used the UNESCO Sea-level Monitoring Facility database (https://www.ioc-sealevelmonitoring.org/) which contains data measured with 1-15 minutes time step, developed to allow for timely analysis of tsunami danger, to analyse high-frequency sea-level oscillations in the Mediterranean basin and relate them to the prevailing atmospheric conditions. This work was subsequently expanded by Vilibić and Šepić (2017) and Zemunik et al.

https://doi.org/10.5194/egusphere-2024-1601
Preprint. Discussion started: 5 June 2024

(2022a, 2022b). The listed papers all focus on the high-frequency component of sea-level oscillations, i.e., all analyses were performed on filtered sea-level series (high-pass filter with cut-off period from 2 to 6 hours, depending on a study), and thus only assess the relevance of high-frequency sea-level oscillations per se, but not in addition to the storm surges. It should be noted that Zemunik et al. (2021a, 2021b) also published a database ("MISELA") in which high-frequency sea-level data (cut-off period of 2 hours) is provided for 331 tide-gauge stations distributed worldwide.

Recently, Ruić et al. (2023) made a step forward, by analysing the contribution of high-frequency sea-level oscillations (T < 2 h) to total, i.e., residual positive sea-level extremes of the Adriatic Sea (Mediterranean; Fig. 1). They used sea-level series measured with a 1-min time step at 18 Adriatic Sea tide gauge stations. Length of series, depending on station, was from 3-17.5 years. The authors have shown that high-frequency sea-level oscillations can give rise to extreme sea-levels of the Adriatic, both independently - meaning that maximum sea-level height is mostly due to high-frequency component, and jointly with a low-frequency component (T > 2 h) – meaning that the maximum sea-level height is due to both the storm surge and short-period oscillations. Their analyses revealed that the contribution of the high-frequency component is largest at stations in narrow channels, and in bays with high amplification factors. The study further found that high-frequency sea-level oscillations can contribute to positive sea-level extremes throughout the year but that their contribution is slightly higher during the warm season (May-September), suggesting that it might be possible to link the oscillations with synoptic weather patterns.

Numerous studies, particularly for the Mediterranean, have shown that the strongest atmospherically induced short-period sea-level oscillations generally occur when particular synoptic conditions prevail over the area. The pioneering studies go back to Ramis and Jansà (1983) for the Balearic Islands and to Hodžić (1988) for the Adriatic Sea. Ramis and Jansà (1983) document a three-layer troposphere during the strong "rissaga" (local name for meteotsunami) which occurred in Ciutadella (Balaeric Islands) on 2 July 1981. A well-mixed, warm and moist shallow surface layer extended to an altitude of ~900 hPa. This layer was overlain by a temperature inversion, followed by a deeper layer, which was warm and dry in its lowest part, but whose temperature decreased with a high rate, and whose humidity and wind speed increased with altitude, possibly leading to conditionally or dynamically unstable mid and upper troposphere layers. On the horizontal scale, a low-pressure trough was located to the west of the Balearic Islands, warm air was advected from the southwest at altitudes higher than 900 hPa (resulting in mentioned temperature inversion), and a front size of a deep upper-level trough was located over the Balearic Islands, with strong mid and upper troposphere south-westerly winds blowing above the islands (Jansà and Ramis, 2021). As for the Adriatic Sea, following The Great Vela Luka tsunami of 21 June 1978, Hodžić (1988) notes that this event and two earlier events occurred during a presence of a weak surface cyclone over the Adriatic Sea, and that strong south-westerly winds in the upper layer were blowing over the Apennines towards the eastern Adriatic. In the following decades, other authors documented similar synoptic conditions over the Balearic Islands, Adriatic Sea and other Mediterranean locations during intense high-frequency sea-level oscillations and meteotsunamis (Jansà et al., 2007; Vilibić and Šepić, 2009; Šepić et al., 2009; Šepić et al., 2015a; Šepić et al., 2015b).

https://doi.org/10.5194/egusphere-2024-1601
Preprint. Discussion started: 5 June 2024

The prevalence of the described synoptic conditions during the “rissagas" on the Balearic Islands led to the development of a probabilistic "rissaga" warning system for Ciutadella as early as 1985 (Jansà and Ramis, 2020). The system was based on the premise that the greater the similarity of forecasted synoptic fields to a characteristic synoptic situation, the higher the probability of a strong “rissaga". Šepić et al. (2016) proposed a quantitative meteotsunami synoptic index that links the average height of short-period sea-level oscillations in Ciutadella to a linear combination of selected synoptic variables (e.g. wind speed and direction in the middle troposphere, horizontal MSLP and temperature gradients, etc.). Both the probabilistic forecast and the index are successful in predicting “no-rissaga/rissaga” conditions – if there is no favourable synoptic pattern, there will be no “rissaga”, if there is a pattern, there could be a “rissaga” - but both are less successful in predicting “rissaga” strength. For the short-period sea-level oscillations to reach their full strength, additional factors are required, i.e. mesoscale atmospheric pressure perturbations, which cannot be resolved by synoptic analyses or forecasts, and which should develop and propagate over the shelf with favourable speed and direction. Such disturbances can only be assessed through high-resolution modelling and real-time observations (e.g., Denamiel et al., 2019).

A plausible explanation on why the described synoptic pattern is favourable for development of high-frequency sea-level oscillations was first suggested by Monserrat and Thorpe (1996) who suggested that given synoptic conditions favour the trapping of atmospheric gravity waves. Once trapped (ducted) atmospheric gravity waves can propagate over the area for a prolonged time without dispersing and can thus act upon the sea long enough to generate strong long ocean waves. Later, it was shown, that in addition to atmospheric gravity waves, convective pressure jumps (for which a statically unstable atmosphere, as the one described above, is also favourable) can also be responsible for generation of intense short-periods sea level oscillations (Jansà et al., 2007; Belušić et al., 2007).

The extraction of synoptic patterns leading to strong high-frequency sea-level oscillations has also been carried out for several other worldwide locations, but the strongest oscillations were nowhere as clearly linked to one synoptic situation as in the Mediterranean Sea. Bechle et al. (2016) used radar reflectivity imagery to classify weather patterns and storm types responsible for the Great Lakes events. They found that 78% of the observed events were due to convective storms, followed by extratropical cyclones and only a small amount was due to atmospheric gravity waves unrelated to storms. Lewis et al. (2023) separated the meteotsunamis in the United Kingdom into “summer-type” and “winter-type” events. The summer events were mostly associated with the advection of warm air from the south and convective precipitation/storms, while the winter events were related to extratropical cyclones. Similarly, Pellikka et al. (2022) also distinguish between “summer-type” and “winter-type” synoptic meteosunami patterns on the Finnish coast. Finnish “summer-type” events were associated with mesoscale convective systems, and with gust fronts; and were found to be concurrent with advection of warm air from the south in the lower troposphere and a strong jet-stream in the middle and upper troposphere. “Winter-type” events were associated with deep extratropical cyclones, and related instabilities and fronts. Rabinovich et al. (2020) also present two general types of meteotsunamis i.e. the “good-weather” and “bad-weather” meteotsunamis. The “good” and “bad” refers to the general state of the atmosphere and ocean during these events. We can argue that “good-weather” meteotsunamis correspond generally to “summer-type” meteotsunamis, and “bad-weather” to “winter-type”.

https://doi.org/10.5194/egusphere-2024-1601
Preprint. Discussion started: 5 June 2024

In this paper we continue the work of Ruić et al. (2023) on high-frequency Adriatic sea-level extremes. We extract and classify atmospheric synoptic situations that lead to the development of extremely strong high-frequency sea-level oscillations along the Adriatic coast by using k-medoid clustering method. One of the initial methods used to order information from large sets of synoptic data was EOF - Empirical Orthogonal Functions (Lorenz, 1956) which looks to decompose the given data into a set of orthogonal functions. These functions aim to capture (explain) the variance of the given data, so the first EOF contains the most variance and each subsequent less and less (Navarra and Simoncini, 2010). This method has been used in various geophysical problems, including sea-level variability (Raicich, 2010), wind field classification (Pandžić and Likso, 2005), global climate (Roundy, 2015), and others. Nowadays, one of the most popular classification methods, are k-means (Hartigan and Wong, 1979) and self-organizing maps, SOM for short (Kohonen, 1984). Both methods group given objects into a predetermined number of clusters using a selected proximity metric, such as Euclidean distance. Both methods, calculate a centroid for every cluster, which is representative of the average of each object (from the training period) inside the given cluster. These centroids are used for labelling new objects (from the testing period) by computing the proximity of the object to them. The "winning" centroid is the one for which this distance is minimal. Although these methods are widely used for this type of analysis, they have some drawbacks. Firstly, the creation of the centroids can be sensitive to outliers especially for k-means method. Secondly, the selected distance metric can lead to wrong labelling of the new objects (from the testing period), especially when atmospheric data is considered, and some objects that would go into the same category, according to the physical process that governs them, get labelled differently (Winderlich et al., 2023. In review).

In this paper we use the k-medoid algorithm (Kaufmann and Rousseeuw, 1987), which also groups objects to a predetermined number of clusters using a distance metric, but it does not create a new object, rather it choses one of the objects from the cluster as a centroid (termed "medoid" in k-medoid method), against which, each new object is compared. Furthermore, rather than the used Euclidian distance metric we use the structural similarity index measure, SSIM (Wang et al., 2004), which forms the clusters based on the similarity of objects. This method shows better results compared to Euclidean distance metric (Wang and Bovik, 2009) and is more resilient to problems associated with outliers and wrong labelling.

We perform the analysis of synoptic conditions for episodes of extreme high-frequency oscillations in the Adriatic Sea. Since this includes both events in which the background sea-level was low and episodes in which it was high (storm surges), we expect to extract at least two types of characteristic synoptic situations – one in which only the high-frequency sea-level oscillations are high, and the other in which the low-frequency component, i.e. the storm surge, is also high.

The paper is structured as follows: Sect. 2 brings materials and methods; in Sect. 3 results are presented and in Sect. 4 the discussion and conclusions are given.

https://doi.org/10.5194/egusphere-2024-1601
Preprint. Discussion started: 5 June 2024

2 Materials and methods

Ruić et al. (2023) analysed sea level series measured with a 1-minute time step at 18 tide gauge stations located along the eastern and western coasts of the Adriatic Sea (Fig. 1). Length of the time series was 3-17.5 years. Prior to the analyses, the authors performed rigorous quality control of all sea level series, removing of all non-physical spikes and outliers. Following this, they extracted "Residual extremes" from the de-tided series. Residual extremes were defined as periods during which sea level was above a certain threshold (99.85 percentile). Contribution of low-frequency and high-frequency sea level to Residual extremes was assessed. The authors also extracted "High-frequency" (HF) extremes – these were extracted from residual series filtered with a 2-hour Kaiser-Bessel window (Thomson and Emery 2014). HF extremes were defined as periods during which high-frequency sea-level component was above a 99.993 percentile threshold. For both types of extreme, a condition stating that two consecutive episodes must be separated by at least three days was enforced.

In Fig. 2 one episode for both types of extremes is shown for the tide gauge Bakar.

Here, we focus on: (i) HF extremes, and (ii) HF extremes which were at the same time Residual extremes. The simultaneous events (HF extreme + Residual extreme) are called Compound extremes from now on. From 18 tide gauge station used by Ruić et al., (2023), we have chosen six with the longest records (16.4-17.9 years) for our analysis. These stations are, in order north-south: Rovinj, Bakar, Zadar, Split, Ploče and Dubrovnik (yellow circles in Fig. 1). For selected stations, information on the HF extremes (date, heights of residual, high-frequency and low-frequency component, for each event) were extracted from Ruić et al. (2023). Basic properties of HF extremes at each station are listed in Table 1. HF extremes were separated into two sets, a training set and a testing set. The training set spans from the start of the measurement, (slightly different for each tide gauge, at the earliest: 1 January 2003; at the latest: 19 June 2003), until 31 December 2017 and the testing set from the 1 January 2018 until 31 December 2020.

Table 1. Locations of tide gauges, length of time series (in years) as well as percentile thresholds (in cm) for defining HF extremes and the number of episodes in the testing and training periods.

https://doi.org/10.5194/egusphere-2024-1601
Preprint. Discussion started: 5 June 2024

Tide gauge	Location	Length of series used [years]	Percentile threshold [cm]	Number of episodes in the training period (2003-2017)	Number of episodes in the testing period (2018-2020)
Dubrovnik	42.65 N, 18.09 E	17.1	5	34	14
Ploče	43.05 N, 17.43 E	17.9	18.4	39	8
Split	43.51 N, 16.44 E	17.4	10	45	11
Zadar	44.12 N, 15.24 E	17.5	10.9	44	10
Bakar	45.37 N, 14.62 E	16.4	21.4	56	8
Rovinj	45.08 N, 13.63 E	16.8	11.1	30	19

Analyses of synoptic conditions were performed by applying k-medoids clustering method to the ERA5 reanalysis data (Hersbach et al., 2020; Copernicus Climate Change Service (C3S), 2017). After initial tests with a range of variables, we focused on the following ERA5 variables: (i) mean sea-level pressure, (ii) temperature at 850 hPa and (iii) geopotential at 500 hPa. The variables were downloaded for the area of the Adriatic Sea (approximate area shown in Fig. 1) for 12:00 UTC of each day of the training and testing period. It should be noted that favourable conditions for generation of strong high-frequency sea-level oscillations can usually be detected in spatial fields of these same synoptic variables (e.g., Jansà et al., 2007; Vilibić and Šepić, 2009; Šepić et al., 2015b).

https://doi.org/10.5194/egusphere-2024-1601
Preprint. Discussion started: 5 June 2024

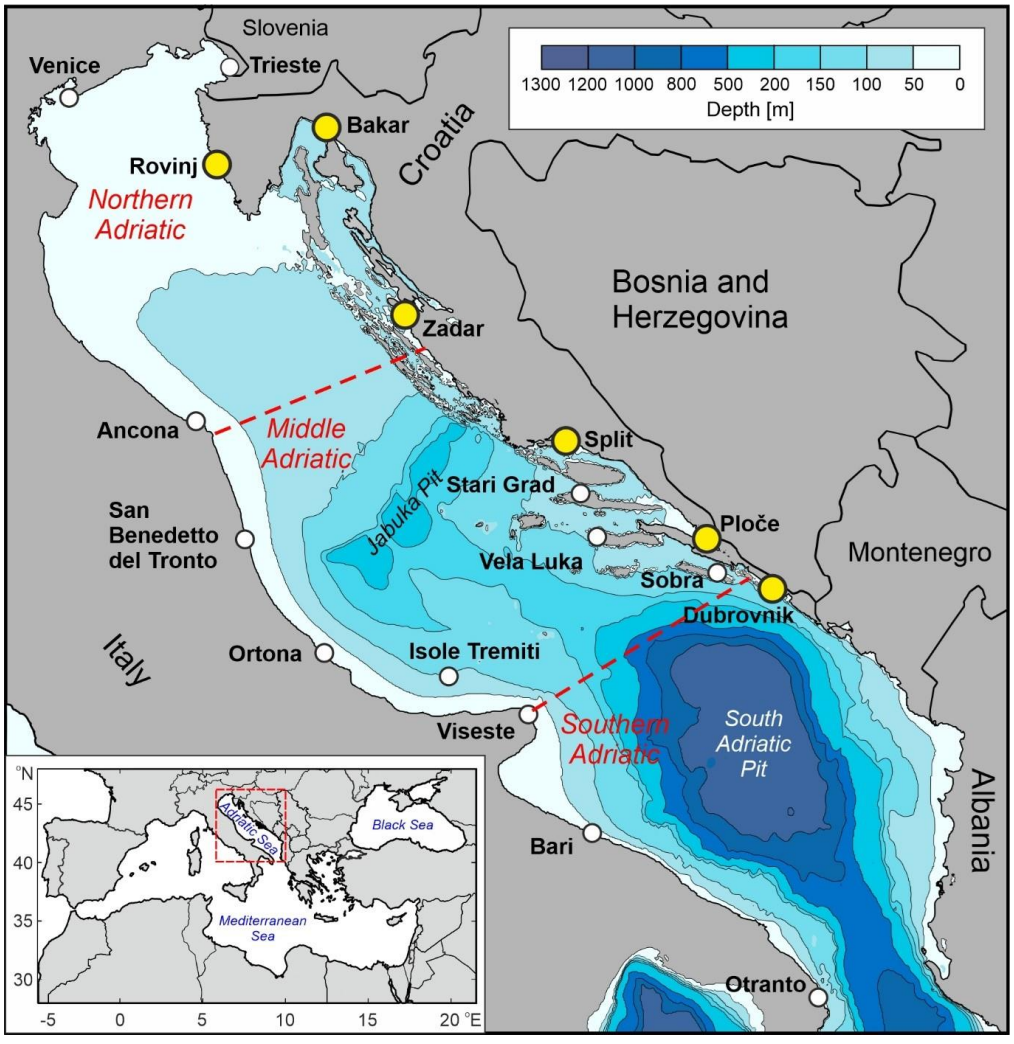

Figure 1. Bathymetry, locations, and names of tide gauge stations (circles) used in Ruić et al. (2023). Coloured yellow circles mark tide gauges analysed in this paper.

For each ERA5 variable, means and standard deviations of each month were calculated using the ERA5 data for the whole period (from 2003 until 2021). For the training period, only days in which HF oscillations occurred were included in analyses. Synoptic data corresponding to each HF extreme of the training period were normalized by subtracting the monthly mean and dividing the resulting series by the monthly standard deviation. All normalized variables (mean sea-level pressure, 850 hPa temperature and 500 hPa geopotential) were concatenated to form one variable/vector (called data point) for each day in which the HF extreme occurred. Clustering was then performed using the k-medoids algorithm. The structural symmetry index measure (SSIM) was used as the distance metric treating the data points, (i.e. concatenated vectors of each

https://doi.org/10.5194/egusphere-2024-1601
Preprint. Discussion started: 5 June 2024

HF event), as images, with different channels (each channel for one of the variables: mean sea-level pressure, temperature and geopotential).

The SSIM was calculated as given by Wang et al. (2004). If *x* and *y* are two variables (e.g., temperature) where *x* represent one and *y* some other HF extreme situation than:

$$SSIM(x,y) = \frac{(2\mu_x\mu_y + c_1)(2\sigma_{xy} + c_2)}{(\mu_x^2 + \mu_y^2 + c_1)(\sigma_x^2 + \sigma_y^2 + c_2)}, \quad (1)$$

where μ_x and μ_y are mean values of *x* and *y* respectively and σ_x and σ_x their variances while the σ_{xy} is the covariance. Lastly, the c_1 and c_2 are the stabilization coefficients that help if the denominator in (1) is close to zero which are computed as $c_{1,2} = (K_{1,2}L)^2$, where *L* is the dynamic range of pixel values and $K_{1,2}$ are small (<< 1) constants (Wang et al., 2004).

Silhouette and Elbow methods were used to determine optimal number of clusters for each station. Silhouette method is used to assess the quality of the preformed clustering in dependence on the number of clusters (Rousseeuw, 1987). For each data point in a cluster, the method takes the average distance of that point from all the other data points in that cluster (denoted as *a*). Then for that same data point it takes the average distance from all the other data points from the next nearest cluster (denoted as *b*). The value of the Silhouette score is then given by: $(b - a)/\max(a, b)$. Higer values indicates better matching of the data point to its assigned cluster and poor matching to the neighbouring cluster. A total silhouette score can be obtained by taking the mean value of each data points score.

Elbow method is another way for finding the optimal number of clusters (Kodinariya and Makwana, 2013) which we applied. It is a visual method since it requires looking at the plot and determining the exact location of the "elbow". To find it, the method computes the sum of square distances (called inertia here) of each data point to the assigned centroid (medoid in our case), within each cluster. By adding more clusters, the inertia is obviously dropping, but the key thing is to find the number (elbow point) after which the drops are less significant.

https://doi.org/10.5194/egusphere-2024-1601
Preprint. Discussion started: 5 June 2024

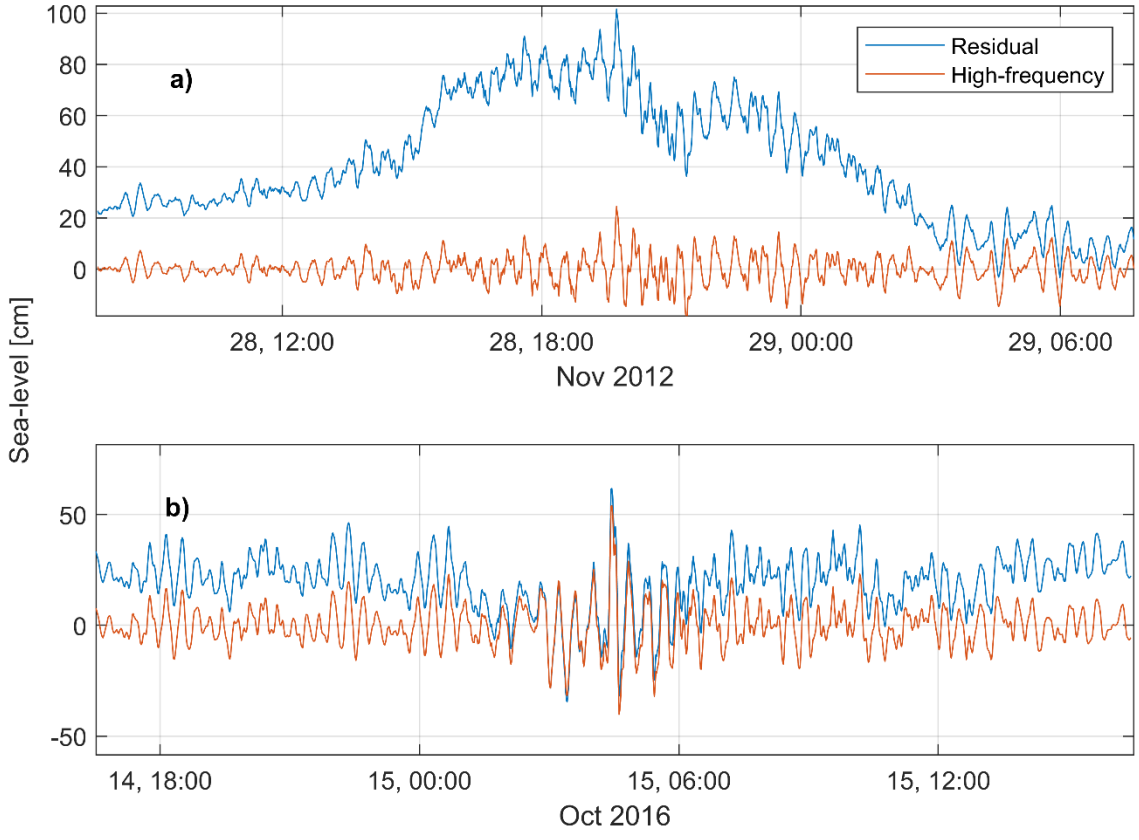

Figure 2: a) Residual extreme of 28 November 2012; b) HF extreme of 15 October 2016.

3 Results

3.1 HF and Compound extremes

As previously stated, we split HF extreme episodes, extracted by Ruić et al. (2023), into two categories: (1) *HF extremes* - episodes with only HF sea-level reached extreme values, and (2) *Compound extremes* - episodes in which both HF and residual sea level reached extreme values. Yearly distribution and heights of both types of extremes are shown in Fig. 3. At some tide gauges, e.g., Bakar and Zadar events are more evenly distributed over the years. At other stations, e.g., Rovinj, events are clearly more abundant in one period (2016-2021) and very rare in other periods (2004-2014). Some events were captured only at one tide gauge station, while others were captured at multiple tide gauges, for instance the *Compound extreme* of 29-30 October 2018 was recorded on stations Rovinj, Bakar, Split, Ploče and Dubrovnik.

The height of HF and Compound extremes is strongly station dependant, as is the contribution of HF component to the total signal. At Dubrovnik, residual height of the sea-level during HF extremes ranges from 5 to 52 cm, and at Bakar

https://doi.org/10.5194/egusphere-2024-1601
Preprint. Discussion started: 5 June 2024

from 4 to 134 cm (Table 1; Fig. 3), whereas height of HF component ranges from 5 to 14 cm at Dubrovnik, and from 21.4 to 54 cm at Bakar. The residual height of the sea-level during Compound extremes ranges from 34 to 52 cm at Dubrovnik, and from 58 to 134 cm at Bakar, with the contribution of HF component from 6 to 12 cm at Dubrovnik, and from 24 to 51 cm at Bakar during Compound extremes. In Rovinj, Bakar, Zadar and Ploče, the HF component can contribute with more than 50% to Compound extremes. On the other hand, in Split and Dubrovnik, this contribution was lower than 30% for all joint episodes.

Monthly distribution of events is shown in Fig. 4. At Rovinj, and Zadar there is a clear seasonal signal with most of the HF extremes recorded from June to August, followed by September and October. Similar signal is present in Ploče and Bakar, but comparable number of events were found in May as well. In Split, the HF extremes peak from April to June, then also in August and in November. At Dubrovnik, number of HF extremes is similar throughout the year – with the second lowest number of HF extremes observed in August – in contrast to most other stations, where August has the highest number of events. Regarding the Compound extremes, at stations Bakar, Split and Dubrovnik, they are clearly shifted towards colder part of the year (October-December; and less January-April), in line with the known distribution of storm surges (Lionello et al., 2012; Ruić et al., 2023). At Rovinj, Zadar and Ploče, the seasonal distribution is less clear. Different seasonal distribution of HF and Compound extremes hints that there are at least two different synoptic situations that can produce strong HF oscillations, one associated with the summer-time conditions (presumably similar to “summer-type”, “good-weather” meteotsunami synoptic situations; Rabinovich, 2020; Lewis et al., 2023; Pellikka et al., 2022) and the other with the fall/winter conditions (presumably similar to “winter-type”, “bad-weather” meteotsunami synoptic situations; Rabinovich, 2020; Lewis et al., 2023; Pellikka et al., 2022).

https://doi.org/10.5194/egusphere-2024-1601
Preprint. Discussion started: 5 June 2024

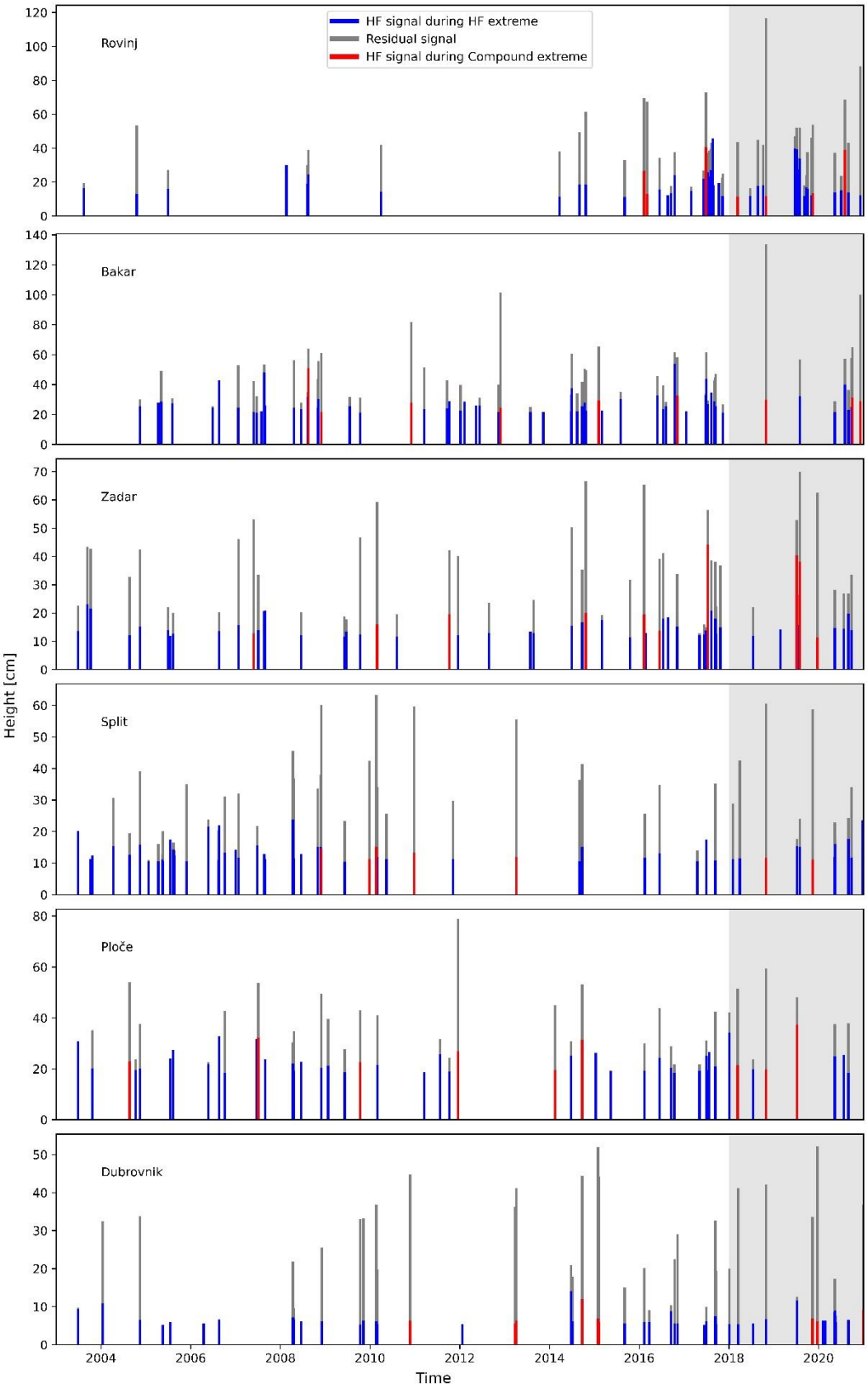

https://doi.org/10.5194/egusphere-2024-1601
Preprint. Discussion started: 5 June 2024

Figure 3: Temporal distribution of high-frequency sea-level extremes at six tide gauge stations. Blue bars denote heights of HF extremes, while grey bars denote residual heights during the HF extremes. The red bars denote heights of HF signal during Compound extremes. The grey shaded area (2018 to 2021) marks the testing period, while the white area marks the training period (2003 to 2018).

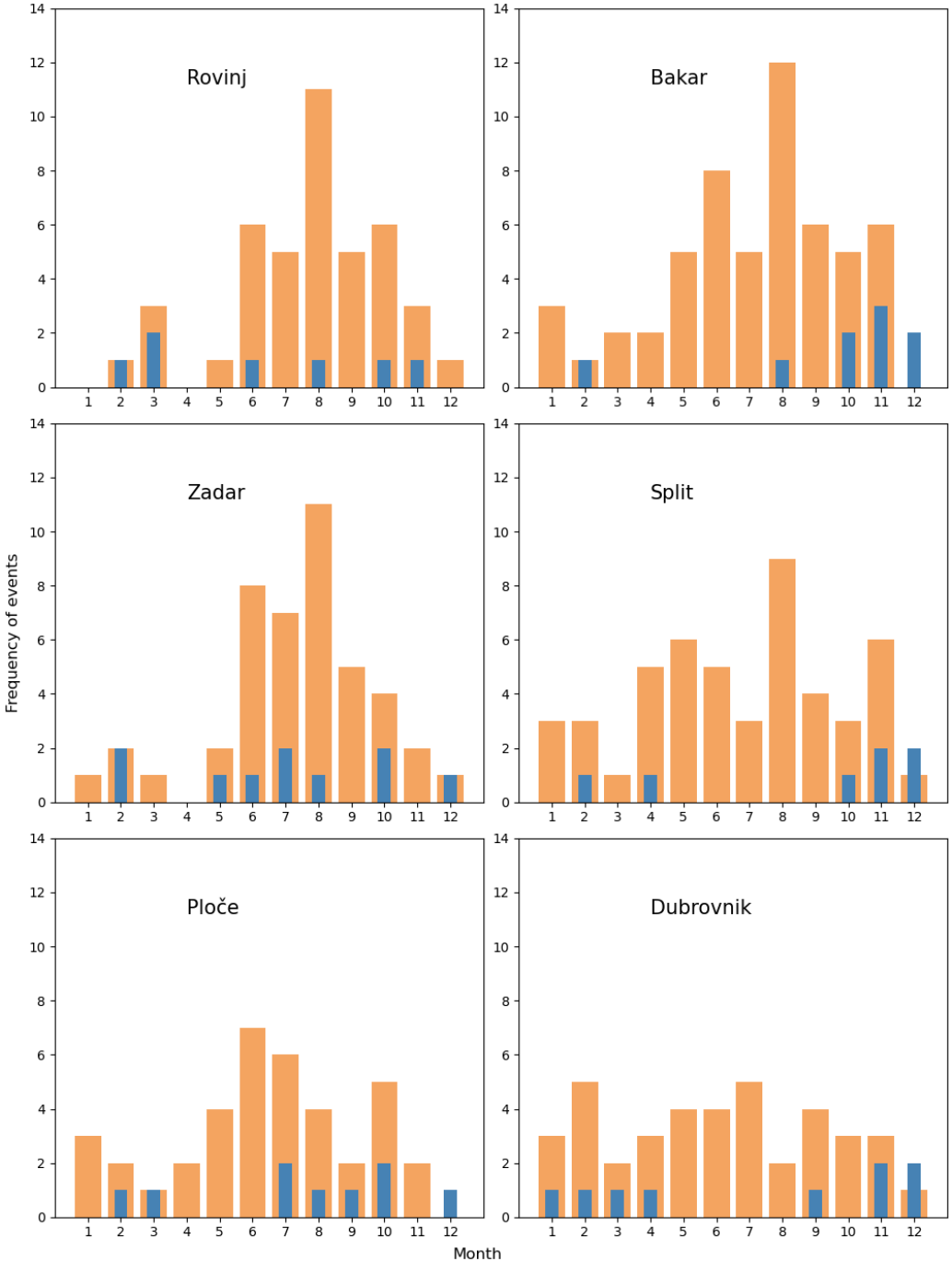

https://doi.org/10.5194/egusphere-2024-1601
Preprint. Discussion started: 5 June 2024

Figure 4: Monthly distribution of the HF (orange bars) and Compound (blue bars) extremes at six tide gauge stations, estimated for the entire period of measurements (2003 to 2021).

3.2 Optimal number of clusters

Before we start with the extraction of characteristic clusters from the training set of episodes, we must determine the optimal number of clusters. The number of clusters is an arbitrary value - thus it can be any number from 1 to total number of episodes, but there are methods for selecting the best number. The two most prominent ones are the Silhouette and Elbow methods described in the Materials and methods. Results of these two methods applied to our dataset are shown in Fig. 5. The first, Silhouette method (Fig. 5a), shows that for most stations highest scores are achieved when 2 to 4 clusters are used, with the optimal cluster number being the one with the highest Silhouette score. For Rovinj, Zadar, Ploče and Dubrovnik the highest score is obtained when two clusters are used. For Bakar, three clusters are the best choice, and for Split, the choice of three or four clusters gives approximately the same score. As for the Elbow method, we are looking for a number of clusters for which the inertia value is low, and for which adding new clusters does not decrease inertia significantly. For all our stations elbow point is located somewhere between 2 and 5 clusters (Fig. 5b). Given the results of Silhouette and Elbow method, we have chosen to apply k-medoids method setting the number of clusters first to 2 and then to 3 clusters, and then to compare results obtained by two choices.

https://doi.org/10.5194/egusphere-2024-1601
Preprint. Discussion started: 5 June 2024

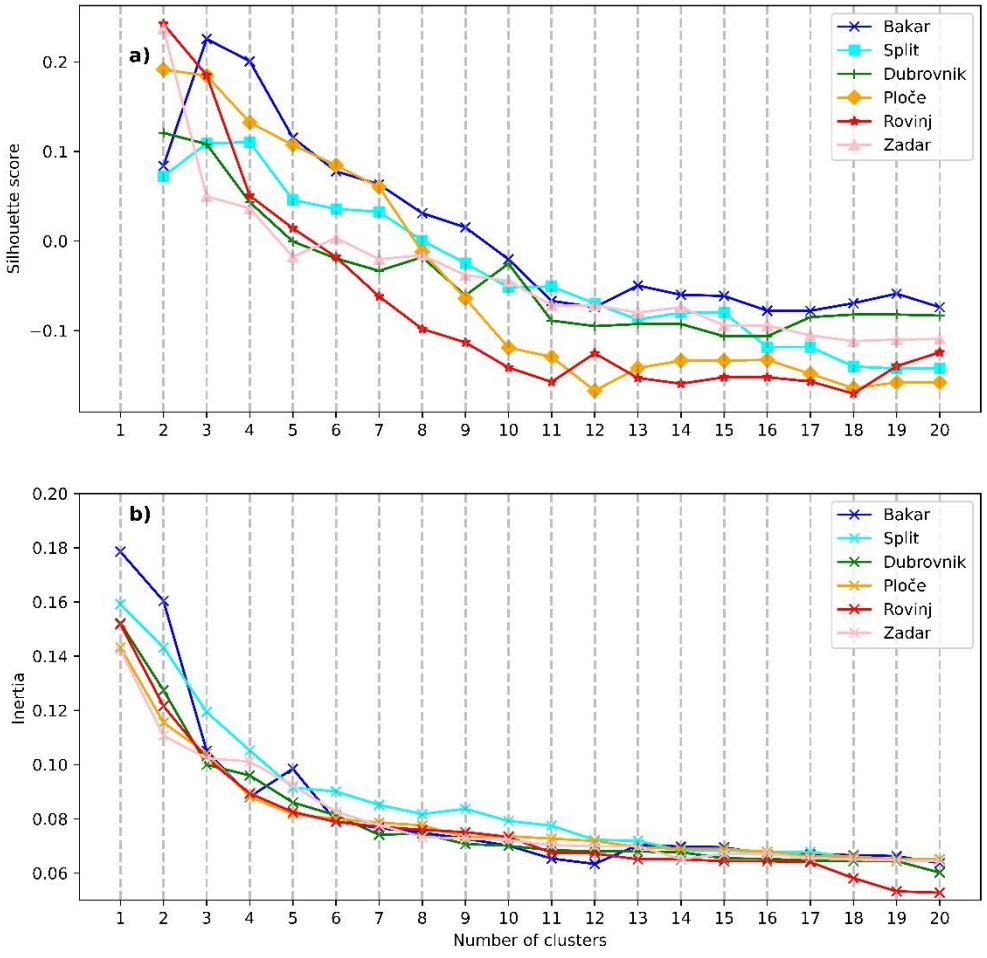

Figure 5: a) Silhouette and b) Elbow methods for determining the number of clusters. Color-coded are the different tide gauge stations.

3.3 Characteristic synoptic patterns

320 Medoids, i.e., representative situations for each cluster, which are defined as episodes which differ the least from all other episodes in each cluster, are presented in Figs. 6-8 (in panes "a)" for 2, and in panes "b)" for 3 clusters. Medoids are shown for Bakar (representative station for the northern Adriatic, Fig. 6), Split (representative station for the middle Adriatic, Fig. 7), and Dubrovnik (representative station for the southern Adriatic, Fig. 8). Characteristic medoids for the other three stations are given in Supplementary material (Fig. S1-S3). In all plots, mean sea-level pressure is shown in the

https://doi.org/10.5194/egusphere-2024-1601
Preprint. Discussion started: 5 June 2024

first row, temperature at 850 hPa in the second row, 500 hPa geopotential height in the third row and in the final, forth row, boxplot of HF and low-frequency (LF) heights (with LF heights defined as difference of residual and HF height) of all episodes assigned to each cluster.

Starting with Bakar, two synoptic situations which are selected as medoids, for the choice of two clusters, are shown in Fig. 6a. The two situations differ most at the surface: situation of 16 September 2017 was characterised by a relatively uniform MSLP field over the Adriatic, whereas on 2 September 2017, a closed low was located over the Bay of Genoa with the MSLP distribution over the Adriatic favourable for the weak southeasterly sirocco winds. Two medoids differ much less at altitudes of 850 hPa, and 500 hPa: an inflow of warm air from the southwest was present at 850 hPa to the south and east of Bakar, and densification of 500 hPa isohypses oriented in southwest-northeast direction was evident over the entire Adriatic Sea on both dates. Observed distribution of the 500 hPa isohypses corresponds to strong south-westerly jet stream of ~25 m/s speed. The jet-stream is an important factor since it steers the atmospheric pressure disturbances that can potentially cause strong HF oscillations. There is no clear distinction between the two medoids. This is also confirmed from box plots shown in the fourth row of Fig. 6a where HF and LF heights of events associated with the specific cluster are presented. It appears that distribution of HF and LF components are rather similar for both clusters. The choice of three clusters leads to three different medoids/clusters (Fig. 6b). Episode on 11 July 2017 resembles the episode of 16 September 2017 (which is one of the medoids obtained for a choice of two clusters). The MSLP was again relatively uniform over the Adriatic, there was an inflow of warm air at 850 hPa (albeit the air was warmer, but this was mostly due to the seasonal changes) with a temperature front over the middle/northern Adriatic, and 500-hPa isohypses were densified over the Adriatic, with the westerly-south-westerly winds blowing over the northern Adriatic (wind speeds of ~20 m/s). Cluster 2 (episode of 11 November 2013, second in Fig. 6b) is unlike any obtained for the choice of two clusters. The surface situation, with an extratropical cyclone centred over the Tyrrhenian Sea, favoured north-easterly to northerly winds over the northern Adriatic (e.i., “bora”, Grisogono and Belušić, 2009). These winds are characteristic for the northern Adriatic and can possibly also induce HF sea-level extremes. At altitude of 850 hPa west-to-east temperature gradient was evident, and at 500 hPa a closed low was located over the Tyrrhenian Sea, resulting in easterly winds of ~10 m/s over the northern Adriatic. The situation on 30 November 2008 somewhat resembles the situation of 2 September 2017 at all layers, but with a clearer distribution of the MSLP favouring sirocco wind and development of storm surge in the northern Adriatic. There was an inflow of warmer air from the southwest at 850 hPa (although naturally atmosphere was significantly cooler in November than in September), and 500 hPa ispohypses were densified and oriented similarly as the ones during 2 September 2017. Choosing three clusters results with separation of episodes according to the height of LF component; median heights of LF are comparable for Cluster 1 (represented by 11 July 2017 episode) and Cluster 2 (11 November 2013 episode), whereas they are significantly larger for Cluster 3 (30 November 2008) indicating that the latter cluster represents situation favourable for development of Compound extremes. Conclusively, for station Bakar three distinct types of synoptic condition that favour intense HF oscillations (the strongest being meteotsunamis) can be recognised: (i) the classic “good-weather” or “summer-type” medoid (representative episodes: 16 September 2017, and 11 July 2017) similar to the

https://doi.org/10.5194/egusphere-2024-1601
Preprint. Discussion started: 5 June 2024

Mediterranean meteotsunami favourable patterns (Jansà et al., 2007; Šepić et al., 2015a)., (ii) the storm-surge medoid, or "bad-weather" or "winter-type", (30 November 2008), (iii) "bora" medoid (11 November 2013). The fact that an additional type of medoid emerged for a choice of three clusters, vs. two clusters, points that for Bakar station, three clusters are a much better choice than two (as already indicated by Fig. 5).

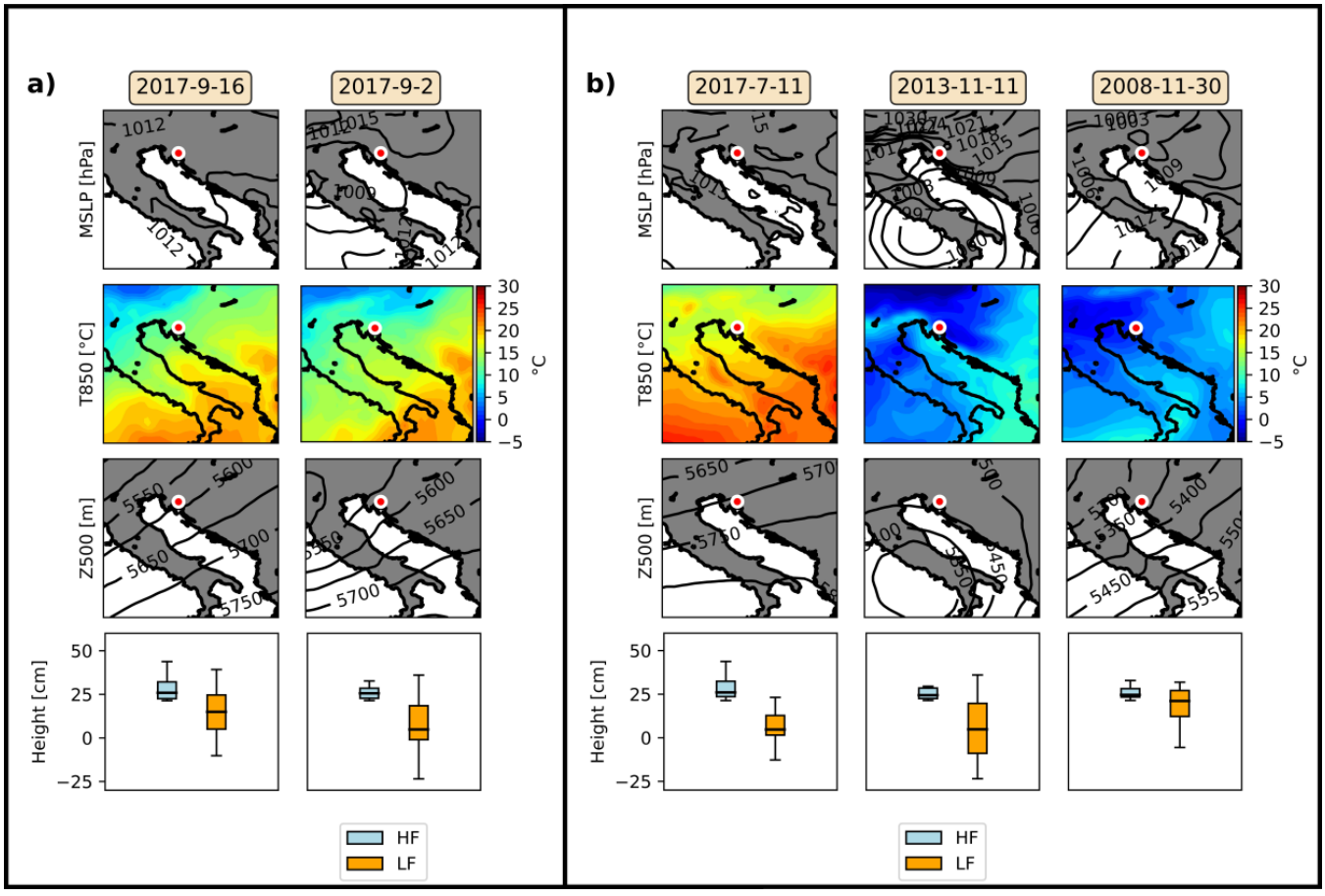

Figure 6: Medoids for the choice of a) two and b) three clusters for Bakar. The first three rows are: mean sea-level pressure (MSLP), temperature at 850 hPa (T850), and geopotential height at 500 hPa (Z). Forth row are the box-plots of HF (blue box) and LF (orange box) heights during the HF extreme episodes assigned to each medoid. The dates of medoids are given at the top of each column and the location of Bakar is marked with a circle.

Characteristic medoids for the choice of two and three clusters for station Split can be seen in Fig. 7 (Fig. 7a for two clusters, Fig. 7b for three clusters). Starting with two clusters, the two medoids differ at all levels. At the surface, on 18 April 2017, a closed low was present over the Tyrrhenian Sea – however, the MSLP gradients were very weak over the middle Adriatic, also leading to weak surface winds, whereas surface situation of 4 October 2006 favoured moderate sirocco winds over the entire Adriatic – with sirocco winds favourable for increase of the LF component. At 850 hPa height, a northeast-to-southwest temperature gradient was evident over the Adriatic on 18 April 2017, and on 4 October 2006, a northwest-to-

https://doi.org/10.5194/egusphere-2024-1601
Preprint. Discussion started: 5 June 2024

375 southeast gradient, similar to the one for most of the Bakar medoids, was evident. At the 500 hPa altitude isohypses were densified over the Adriatic for both episodes, albeit their orientation was slightly different: on 18 April 2017 westerly-north-westerly winds blew with speeds of ~23 m/s blew over the area, and on 4 October 2006 south-westerly winds with speed of ~16 m/s. Box-plot distributions of HF and LF component during extremes grouped in two clusters indicate that Cluster 2 (4 October 2006) represents a situation which is more favourable for development of Compound extremes (higher LF
380 component), whereas Cluster 1 (18 April 2017) represents a "good-weather" situation (lower LF component, weaker surface winds). Looking at the three-cluster choice (Fig. 7b), the first two medoids (7 June 2009 and 22 October 2003) are similar at all levels: weak MSLP gradients leading to weak sirocco winds were present over the Adriatic Sea on both dates; at 850hPa warm air was advected from the southwest, resulting in a high temperature gradient over the middle Adriatic, and 500-hPa isohypses were densified and oriented in southwest-northeast direction leading to wind speeds of ~30 m/s, for both dates.
385 Distributions of HF and LF oscillations are similar for both clusters, although the cluster represented by the medoid of 22 October 2003 has larger median values of LF oscillations (but also broader range). Both medoids resemble the "good-weather" situation. The third medoid (27 November 2005) was associated with a much lower MSLP over the Adriatic Sea with moderate southeasterly sirocco winds blowing over the southern and middle Adriatic, thus favouring development of Compound extremes, which include higher background sea-levels and potentially a storm surge. At higher atmospheric
390 levels, a colder air was advected to the Adriatic Sea from the west, and slightly warmer from the southwest – in a cyclonic circular motion, and at 500-hPa, isohypses were again positioned in a way that favours strong south-westerly winds (with speeds up to 30 m/s). Furthermore, the distribution of LF oscillations reveals highest median and maximal values of all three clusters. Conclusively, two characteristic synoptic situations for generation of strong HF oscillations in Split were extracted, one which is related to "good-weather" (representative episodes: 18 April 2017, 7 June 2009, 22 October 2003) and one
395 which is related to "bad-weather", storm-surge conditions (representative episodes: 4 October 2006, 27 November 2005). Increase of number of clusters from 2 to 3 led to refinement of the "good-weather" cluster.

https://doi.org/10.5194/egusphere-2024-1601
Preprint. Discussion started: 5 June 2024

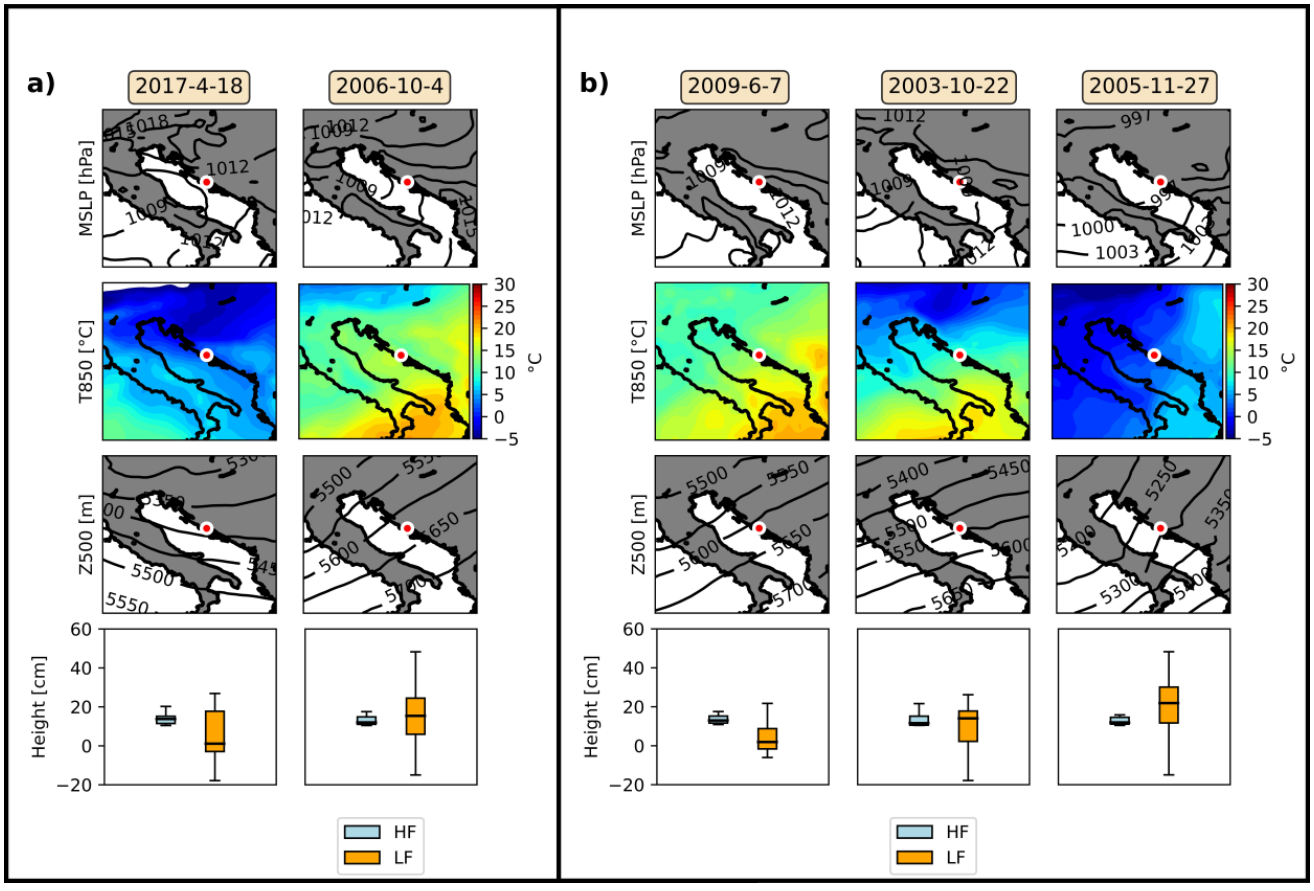

Figure 7: Medoids for the choice of a) two and b) three clusters for Split. The first three rows are: mean sea-level pressure (MSLP), temperature at 850 hPa (T850), and geopotential height at 500 hPa (Z). Forth row are the box-plots of HF (blue box) and LF (orange box) heights during the HF extreme episodes assigned to each medoid. The dates of medoids are given at the top of each column and the location of Split is marked with a circle.

Shifting our attention to the southern Adriatic we can see the medoids, for 2 (Fig. 8a) and 3 (Fig. 8b) clusters, for the station Dubrovnik. Looking at pane a) we again notice the two different patterns: although both medoids were characterised by uniform MSLP over the Adriatic Sea, during the episode of 11 February 2016, a weak to moderate MSLP gradient was present to the south of Dubrovnik and Otranto – leading to south-easterly sirocco winds over the Ionian Sea and the southern Adriatic. At 850 hPa altitude, warm air was advected from the southwest on 5 September 2019, whereas a north-to-south temperature gradient was present over the area on 11 February 2016. Isohypses of the 500 hPa pressure level had different orientation during two episodes, with south-westerly winds with speeds of ~23 m/s blowing on 5 September 2019, and westerly winds of ~26 m/s on 11 February 2016. The two medoids are clearly separated by contribution of LF component to extremes. LF component is significantly larger for events belonging to the Cluster 2, i.e., to cluster represented by 11 February 2016 medoid. Out of the two situations, the 5 September 2019 one resembles more a "good-weather", and the second one is more similar to a "bad-weather" situation, with the latter favourable for Compound extremes. Looking at

https://doi.org/10.5194/egusphere-2024-1601
Preprint. Discussion started: 5 June 2024

the Fig. 8b., in which three medoids are shown, we can see that the first two medoids are the same events as the medoids when the choice of cluster number was two. This can lead us to the conclusion that these two medoids represent the training set of events very well so that even the increase in cluster number does not lead to their change. The last medoid in Fig. 8b) is for situation of 6 November 2009 during which a low-pressure centre was located over the middle Adriatic resulting in alongshore and onshore winds at Dubrovnik coast. At 850 hPa level there was again advection of warm air from the southwest, and at 500hPa isohypses were oriented in southwest-northeast direction, with south-westerly winds with speeds of ~30 m/s blowing over the southern Adriatic. Box-plot distribution of HF and LF heights during the extremes reveals that the third cluster (medoid of 6 November 2009) contains the episodes with the highest LF signal. Conclusively, and similar to Split, there are two characteristic situations for occurrence of strong HF oscillations in Dubrovnik, one associated with the "good-weather" (5 September 2015 as a representative episode), and the other associated with "bad-weather" (representative episodes: 11 February 2016, 6 November 2009). Increase of number of clusters from 2 to 3 leads to a refinement of the "bad-weather" cluster.

Characteristic medoids of the other three station, Rovinj, Zadar and Ploče, are given in the Supplementary material, Figs. 1S-3S. For station Rovinj (Fig. 1S) a distinction between the "good" and "bad" weather conditions is noticeable when choosing the two-cluster approach which is supplemented with an additional "bad-weather" medoid when changing the number of clusters from two to three. This newer medoid (13 November 2017) has similar characteristics to the "bora" medoid of Bakar. The station Zadar has, when looking at the two-cluster choice (Fig. 2Sa), the "good" and "bad" weather medoids, with the "good-weather" situation getting refined when increasing the number of clusters (Fig. 2Sb). The clusters of the final station, Ploče are also separated to "good-weather" and "bad-weather" situations, when number of clusters is set to two. An increase to 3 clusters results in the same two medoids selected as representative ones (also the case for Dubrovnik) (Fig. 3Sb), and a new medoid which represents the refinement of a "bad-weather" medoid. For the three stations shown in the Supplementary material, distributions of HF and LF components during the extremes are in line with "good-weather" and "bad-weather" situations, with higher LF components found in "bad-weather" situations. "Bad-weather" situations are generally more favourable for Compound extremes, and "good-weather" situations for HF extremes.

https://doi.org/10.5194/egusphere-2024-1601
Preprint. Discussion started: 5 June 2024

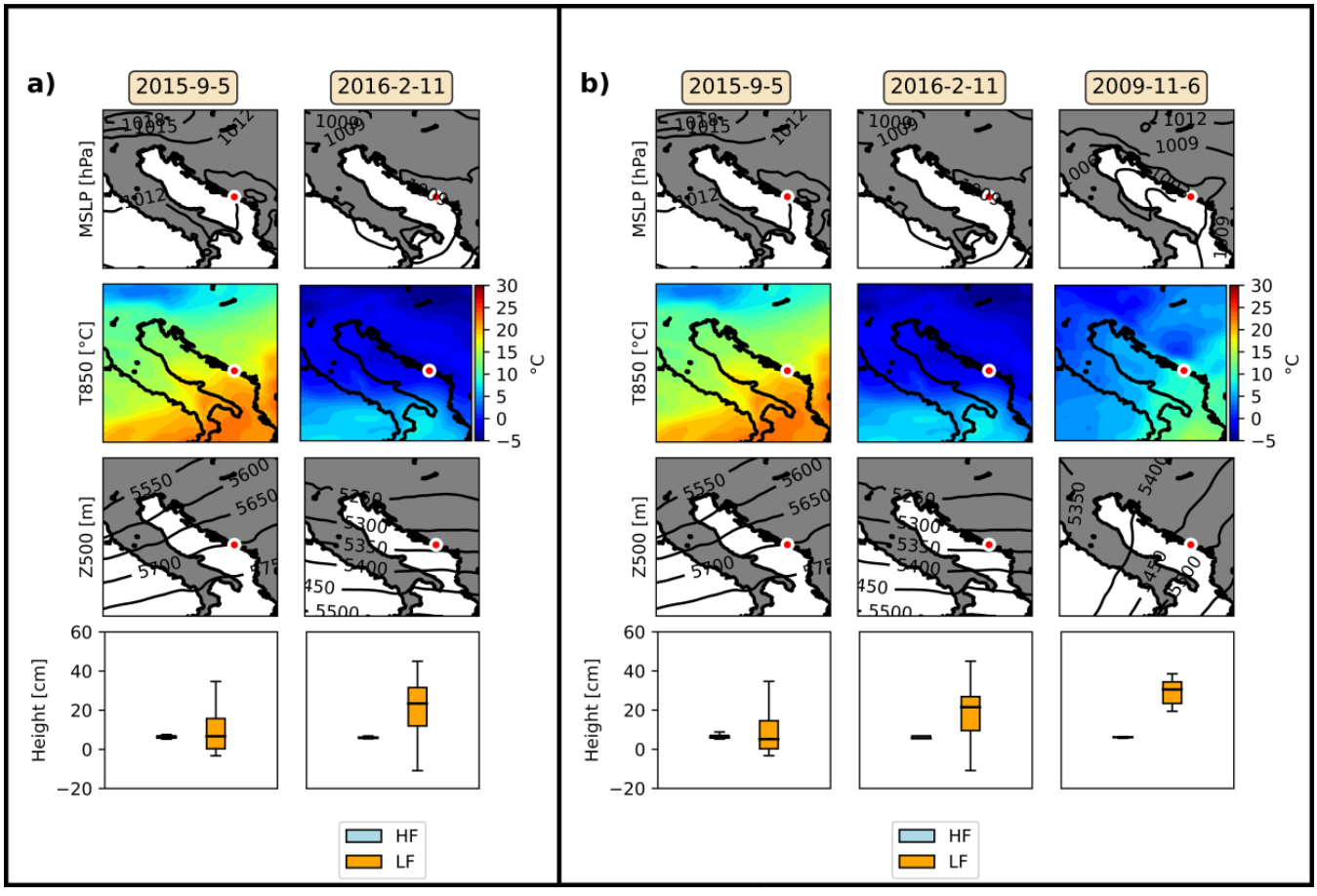

Figure 8: Medoids for the choice of a) two and b) three clusters for Dubrovnik. The first three rows are: mean sea-level pressure (MSLP), temperature at 850 hPa (T850), and geopotential height at 500 hPa (Z). Forth row are the box-plots of HF (blue box) and LF (orange box) heights during the HF extreme episodes assigned to each medoid. The dates of medoids are given at the top of each column and the location of Dubrovnik is marked with a circle.

In Fig. 9 we show monthly distributions of number of episodes within clusters for each station, and for both choices of number of clusters (2 vs. 3; Fig 9a vs. Fig 9b). For station Rovinj the medoid associated with Cluster 1 is more common in summer months (June to August) while the medoid associated with Cluster 2 is more common in colder part of the year. Changing the cluster number from two to three (Fig. 9b), we notice that the events labelled as most similar to the third medoid occur in the same months as medoid number two – however, as seen from Fig. S1, these do not represent a refinement of the "bad-weather" situation, but an addition of a new "bora" situation. Similar conclusions can be reached for stations Ploče and Dubrovnik: already for a choice of two clusters, episodes are separated depending on the season, whereas the addition of a third cluster refines "bad-weather" situations, i.e., situations more characteristic for the colder part of the year. At Zadar, two cluster choice leads to the Cluster 1 occurring in summer months (June-September) while the Cluster 2 occurs mostly in the colder part of the year, peaking in September-November. Adding a third cluster leads to the refinement of the "good-weather" cluster. On the other hand, at Bakar and Split when two clusters are chosen, both appear throughout

https://doi.org/10.5194/egusphere-2024-1601
Preprint. Discussion started: 5 June 2024

the year. Although, in Bakar Cluster 2 is somewhat more common in the warmer part of the year, and Cluster 1 in the colder part of the year. On the other hand, in Split, Cluster 1 appears evenly throughout the year (expect for March), whereas Cluster 2 has rather randomly distributed peaks (in April, August and November). At both stations, adding a new cluster results in a clear seasonal distribution. In Bakar three characteristic seasonal distributions emerge: the "good-weather" cluster, then a "bad-weather", storm surge favourable cluster, and an additional cluster which introduces a "bora" favourable situation (Cluster 2). In Split a new cluster represent a refinement of the "bad-weather" situation.

Observed seasonal distributions are in line on what is known with climatology of weather patterns over Croatia: calm weather conditions are predominant in summer, extratropical cyclones leading to surges peak in autumn but also happen in winter (December to February), and bora conditions peak in January and February (Lionello et al., 2012).

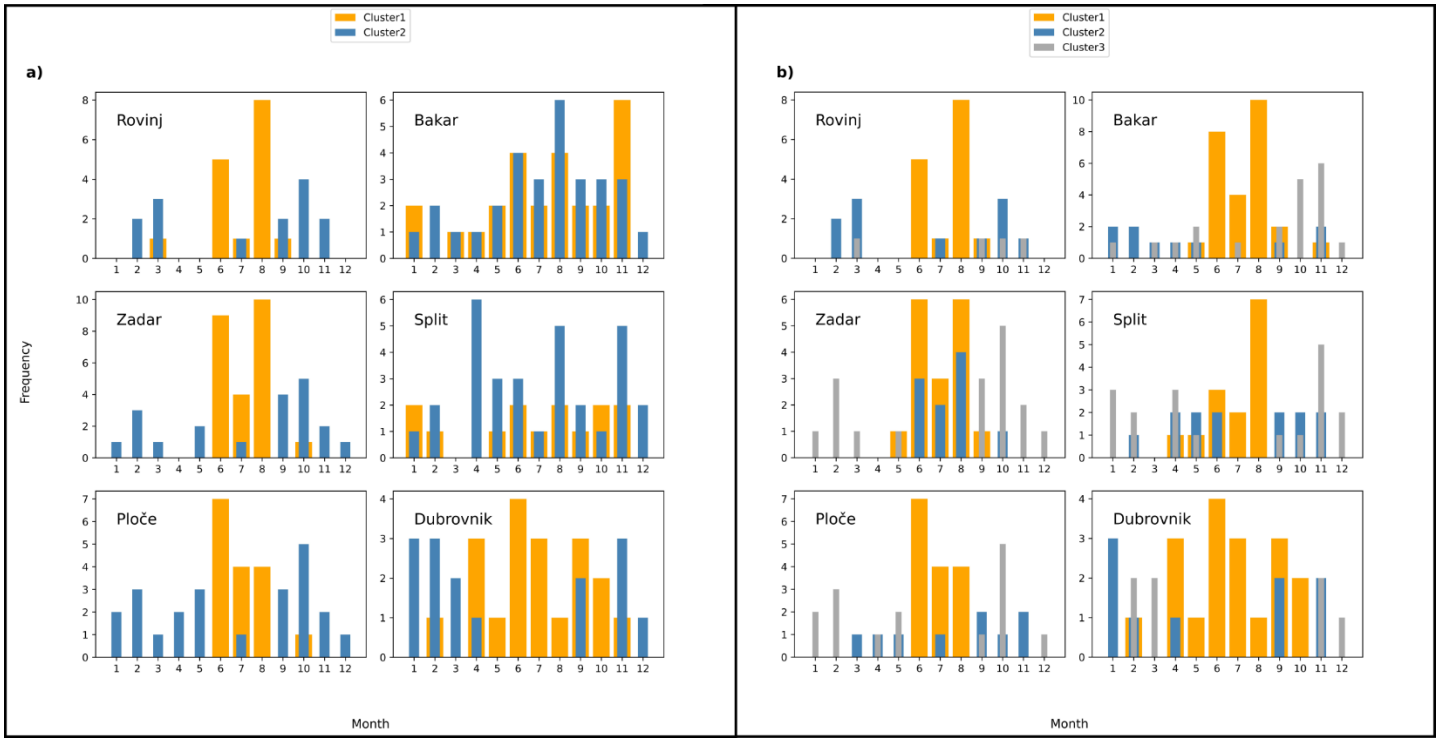

Figure 9: Monthly distribution of cluster labels for each event in the training part of the data set.

3.4 Testing period

For the analysis to be complete, there needs to be a testing period for which the quality of classification is evaluated. The quality of the predictions should help us to assess have all the physical process, responsible for the intense HF oscillations, been captured with the medoids, and to again verify the optimal number of clusters for each station. For each day of the testing period, for each station, and both for choice of two and three clusters, daily synoptic situations (defined as normalised fields of: MSLP, temperature at 850 hPa, and 500-hPa geopotential height at 12:00 UTC of each day) were

https://doi.org/10.5194/egusphere-2024-1601
Preprint. Discussion started: 5 June 2024

compared to characteristic medoids (as extracted from training period, Figs. 6-8 and 1S-3S). Each day was assigned to one of the clusters, depending on the SSIM value, i.e., on difference of synoptic situation of that day and synoptic situation of the representative medoids. Box-plots of the resulting SSIM distributions for each day of the testing period, each cluster, and each station are shown in Fig. 10. In all plots, black dots represent days in the testing period in which an extreme HF event occurred (based on Ruić et al., 2023). Looking at the plots, almost all events in the testing period occur for the SSIM above the 75th percentile value (upper edge of boxes), and all (but 4) for the SSIM above median value. This implies that even for a choice of two clusters, k-medoid method, extracts characteristic patterns for generation of extreme HF oscillations well. Nonetheless, there are clearly stations for which a third and possibly a fourth cluster should be added. Results are further summarized in Table 2. The values of median SSIM for all days in the testing period range from 0.485 to 0.574 for the choice of two clusters and from 0.522 to 0.603 for the choice of three clusters. Since these numbers include all days, with or without a HF episode, the more important metric should be the SSIM median values estimated only for days of extreme episodes. The related SSIM medians range from 0.673 to 0.76 for a choice of two clusters and from 0.682 to 0.748 for a choice of three clusters.

At Zadar and Rovinj SSIM median values for extreme episodes drop when number of clusters increases, as well as the number of episodes with SSIM scores above the 75th percentile (Table 2). This all points to the fact that an additional, third, cluster is not necessary to adequately represent synoptic situations related to extreme HF oscillations at these 2 stations. At Zadar there is one episode that could be considered an "outlier", regardless of the number of clusters, that "scores" very low. This situation is characterised by exceptionally strong sirocco winds blowing over Zadar accompanied with low, gradient free, temperature at 850 hPa and a visible cyclone in the Ionian Sea in the geopotential height at 500 hPa. This situation differs a lot from the medoid ones at Zadar visible in Fig. 2S.

For station Bakar and Split, for which the previous analysis has shown the need for three clusters, the exact opposite is visible. The values of SSIM median for extreme episodes rise when changing from two to three clusters and the percent of episodes above the 75th percentile increases for Split. At station Bakar, for the choice of two clusters, all HF events occur during days that are characterised with SSIM above the 75th percentile, except for one event in cluster 1 for which SSIM value is slightly above the median. In Split, all events, but one, were above median value, with most of them above 75th percentile as well. For the choice of three clusters, in Bakar, all HF extreme episodes had SSIM higher than 65th percentile. For station Split, since two episodes remained below median value when the choice is three clusters, one even below 25th percentile, it might be beneficial to choose one more cluster. This was already hinted in Fig. 5a, as the Silhouette score was approximately the same for the choice of three and four clusters for Split.

At the final two stations (Dubrovnik and Ploče) an increase in SSIM median for extreme episodes occurs, but the percent of episodes above the 75th percentile drops at both stations, when making the change from two to three clusters (Table 2). We should keep in mind that number of events in testing periods ranges from 8 (Ploče) to 19 (Rovinj) and that more events should be considered to get robust statistics.

https://doi.org/10.5194/egusphere-2024-1601
Preprint. Discussion started: 5 June 2024

Table 2. For each cluster number choice (two and three) first column is the SSIM median value of each day in the testing period regardless of the cluster in which the day is put; second column SSIM median value for each day that had the HF extreme event; third column presents the total number of synoptic situations during extreme episodes for which SSIM was above the 75th percentile regardless of the cluster label.

Tide gauge	Two cluster choice			Three cluster choice		
	SSIM median	SSIM median for episodes of extremes	Percent of episodes above the 75th percentile	SSIM median	SSIM median for episodes of extremes	Percent of episodes above the 75th percentile
Dubrovnik	0.574	0.673	64	0.603	0.682	57
Ploče	0.543	0.729	75	0.548	0.746	64
Split	0.521	0.717	64	0.528	0.743	82
Zadar	0.561	0.76	80	0.522	0.741	60
Bakar	0.485	0.722	87	0.579	0.748	75
Rovinj	0.548	0.749	84	0.597	0.728	58

https://doi.org/10.5194/egusphere-2024-1601
Preprint. Discussion started: 5 June 2024

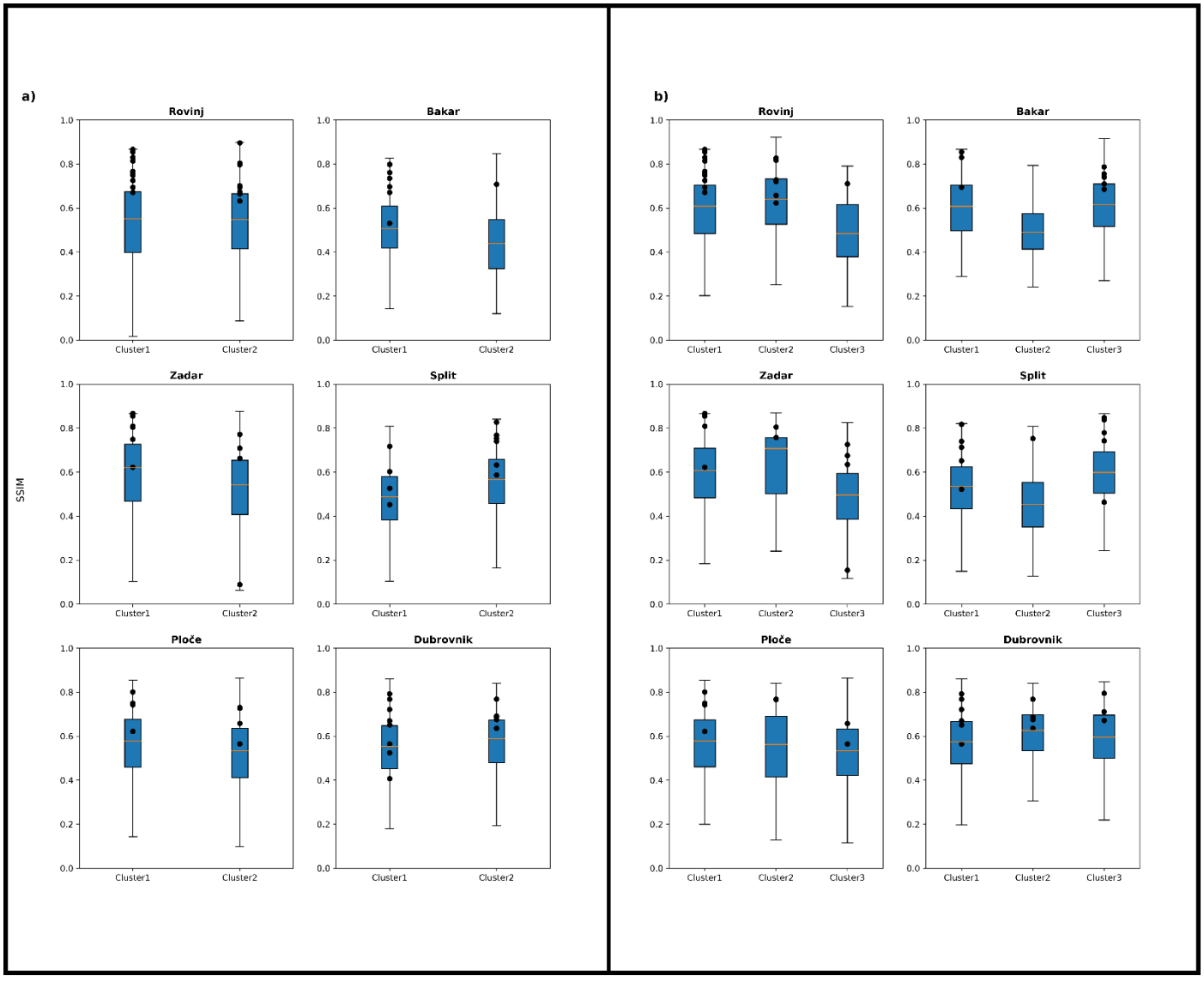

510 **Figure 10: Box-plots of SSIM values at each day of the testing period, in dependence on the assigned cluster. Plots are for each station and the choice between two (left pane) and three (right pane) clusters. Black dots indicate dates of the testing period which contain episodes of extreme HF oscillations (both HF and Compound extremes). In the box-plots, orange lines stand for median values, while the upper and lower edge of the blue box denote the 75th and 25th percentile value, respectively. The whiskers denote the minimum and maximum values.**

515

https://doi.org/10.5194/egusphere-2024-1601
Preprint. Discussion started: 5 June 2024

4 Discussion and conclusions

The general synoptics responsible for producing the strongest HF sea-level oscillations (called meteotsunamis) are already known, especially for the Mediterranean and the Adriatic Sea (e.g., Šepić et al., 2015a). More than a few case studies of strong meteotsunami events have been conducted, confirming the existence of specific meteotsunamigenic synoptic conditions (Vilibić and Šepić 2009; Pupić Vurilj et al., 2003; Šepić and Orlić 2024), which are more likely to occur in the summertime. This in turn leads to frequency of meteotsunamis (and intense HF sea-level oscillations in general) being larger in the summer (Ruić et al., 2023). On the other hand, intense HF sea-level oscillations also occur during other parts of the year when the synoptic conditions are different than in the summertime. Strong HF oscillations can happen jointly to other events such as storm surges. This was the case for the flood of Venice of 12 November 2019 when, during a storm surge, an additional meteotsunami (albeit of a period longer than 4 hours) struck Venice, resulting in a sea-level rise of 182 cm and the flooding of almost the entire city (Ferarrin et al., 2021). Because of these two distinctly different scenarios in which destructive meteotsunamis occur they have previously been separated into “good-weather” and “bad-weather” (Rabinovich, 2020), or “summer-type” and “winter-type” events (Pellikka et al., 2022; Lewis et al., 2023).

To find the exact number and characteristics of meteotsunamigenic synoptic conditions both subjective and objective approaches can be implemented. The subjective approach requires an observer who manually classifies the synoptic situations based on previous experience and gained knowledge. This approach can be useful for the first hand, but because the classification criteria are observer dependant, the results can vary between observers. Furthermore, this approach becomes more difficult as the data set gets larger. On the other hand, the objective approach uses mathematical methods for classification, thus diminishing the big data set problem. This method is not immune to the subjectivity problem, i.e., the subjectivity of the observer can still be partially present in the choice of the mathematical method used to tackle the problem. This can be elevated by testing different methods and finding the optimal one for each problem. The most popular methods for classification are EOF, k-means, and SOM which have been used to classify various problems in atmosphere physics such as the North Atlantic climate variability (Reusch et al., 2007), synoptic and local-scale wind patterns in Tyrrhenian coastal area (Di Bernardino et al., 2022), reconstruction ocean surface temperature and salinity (Elken et al., 2019) and many other.

The k-means and SOM classification methods are known to generate good results but have some underlying problems which need to be kept in mind. Mainly, the centres of clusters are mean values of each cluster element (object), potentially not recognizing the physical processes that are driving the events in each cluster or losing some valuable information about the synoptic state through averaging. On top of that, regarding this particular problem, a low number of events in the training set (a few dozen per station) can represent a problem for k-means and SOM algorithms. The commonly used distance metric in k-means and SOM is Euclidian distance which takes point to point distances, occasionally leading to misleading results. E.g., sometimes, a pressure low separated by only a few points, in two events, will give a large Euclidian distance, although physically the two situations are rather similar (we are more interested in gradients associated to the low,

https://doi.org/10.5194/egusphere-2024-1601
Preprint. Discussion started: 5 June 2024

than to the exact value of the low). These issues can be somewhat overcome by using different normalizations on the input data which can help improve the methods (Milligan and Cooper, 1988). An extra problem arises when the input data is chosen to be a compound of different variables. This enlarges the dimensionality of input data and requires a lot more events for SOM and k-means to be trained effectively.

The issue of large dimensionality and small number of training events can be efficiently resolved by using the k-medoid algorithm that choses specific events (medoids) rather than average values, to represent clusters. By doing this, there can be only a few events inside a cluster and the physical process, which are in the background of each event, can be discussed by examining the characteristic medoid. The problem of the distance metric is amended by using the structural similarity index measure (SSIM) which treats input fields as images (Hoffmann et al., 2021) ensuring that similar synoptic situations get grouped accordingly. The proof of this can be seen in Fig. 12 where all three methods (k-means, SOM and k-medoid) are first used to find clusters in the training set, and then to label (associate to a cluster) all days in the testing period. For the k-means and SOM Euclidian distance was used and for k-medoid method the SSIM was used as the distance metric. Black dots represent days in the testing period in which an extreme HF event occurred. The y-axis has the normalized distances, i.e., the smaller the value the closer (more similar) is the day to its cluster center or medoid. This analysis is presented for station Bakar and both for the selection of two and three clusters. Looking at k-medoid, (green box-plots), it is observed that, almost all the events (black dots) happen when the normalized distance is small in comparison with the other two methods. For the k-means method, both for the choice of two and three clusters, the events happen with no clear connection to normalized distance, they happen when it is large (above the 75^{th} percentile) and sometimes when it is low (beneath the 25^{th} percentile). The same thing can be said for SOM which has, for one cluster, events that happened when the normalized distance was extremely large and events for which it was extremely low. Conclusively, we can say that out of the three tested methods, k-medoid works the best in our situation.

https://doi.org/10.5194/egusphere-2024-1601
Preprint. Discussion started: 5 June 2024

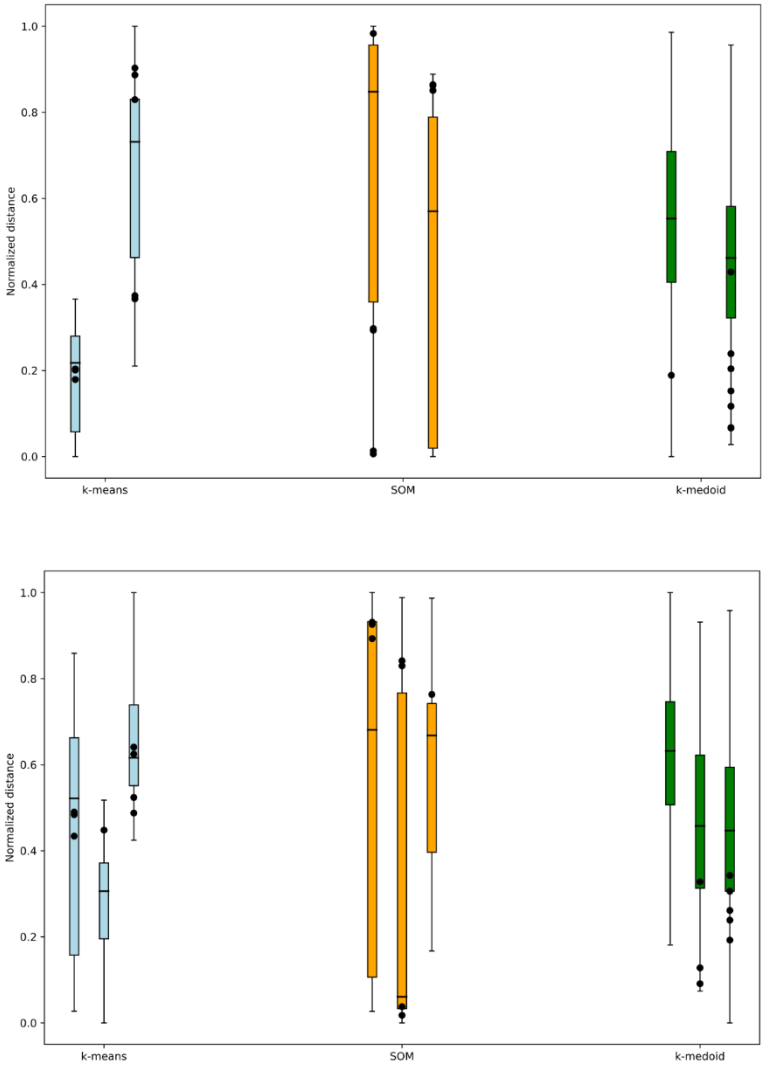

Figure 11: Box-plots of normalized distances of each day in the testing period from the assigned cluster for the choice of two and three clusters. Black dots represent the days in the testing period when HF extreme events occurred. The analysis was carried out for three methods, k-means, SOM and k-medoid for tide gauge Bakar.

The first assumption, that there is a minimum of two distinct synoptic conditions during which intense HF oscillations occur, has proven to be a fairly good one. For most stations (Rovinj, Zadar, Ploče and Dubrovnik) the selection of two clusters splits the training set into a "good-weather" medoid and a "bad-weather" medoid, as seen in Figs. 8, 1S-3S. The "good-weather" cluster is alike to the aforementioned meteotsunami favourable synoptics (wind speed and direction in the middle troposphere, temperature gradient, etc.) which favours the development of ducted atmospheric gravity waves and

https://doi.org/10.5194/egusphere-2024-1601
Preprint. Discussion started: 5 June 2024

convective instabilities which can create intense HF sea-level oscillations. The "bad-weather" cluster describes synoptic settings favourable for storm surge generation (presence of a low-pressure system and sirocco wind) with the possibility of creating pressure jumps associated with the instabilities on the fronts which can also be a trigger for HF oscillations. The monthly distributions of these two clusters (for each tide gauge of the four mentioned) in Fig. 9 resemble the distribution of the HF extremes and Compound extremes presented in Fig. 4. This indicates that the quality of classification algorithm is satisfying. The "bad-weather" clusters have distributions similar to the distribution of Compound extremes in which the LF signal is normally stronger, and "good-weather" clusters have distributions similar to the HF extreme ones in which LF signal is usually lower. The addition of a third cluster, for these four stations, does not produce a significantly different synoptic class, but helps in refinement of either the "bad-water" or "good-weather" situations.

For the last two stations, Bakar and Split, choosing two clusters does not end up with the monthly distribution of clusters (Fig. 9) similar to distribution of HF and Compound extremes in Fig. 4. For Bakar, a choice of two clusters, leads to recognition of two September episodes as cluster medoids, while the increase from two to three clusters gets medoids from different part of the year and with different physical properties. The first medoid now represents a typical meteotsunami favourable situation, the second represents storm surge favourable condition, and the third one the bora wind synoptic setting. The bora wind medoid present a newer finding which was not visible for the previous stations, except for Rovinj, revealing an additional process that can induce intense HF sea-level oscillations. For station Split, there is no clear addition of a newer physical process when number of clusters is changed from two to three clusters (Fig. 7), but the seasonal signal is clearer when number of clusters is larger (Fig. 9). Additionally, in Fig. 5 the optimal number of clusters for Split can be argued to be four or even five meaning that maybe adding an extra cluster would result in revelation of additional processes. Nonetheless, we stopped our analysis with three clusters because in the testing period, almost all the days with the HF extreme were labelled as very similar to one of the clusters as seen in Fig. 10.

We are left to discuss a potential for application of this method for forecasting the intense HF sea-level oscillations. There are at least two different approaches to generating forecasts of intense HF oscillations. The first approach involves incorporating this method into another one, e.g., neural network method, or using it alongside atmospheric and oceanographic models to make predictions. The second approach involves using this method alone to get fast predictions of the HF sea-level oscillation heights. Firstly, lets focus on the combination of the presented method with a neural network or an oceanographic model. The neural network meteotsunami forecast system was already tested for the Balearic Islands (Vich and Romero, 2021). That forecast system has shown good results in predicting rissaga and non-rissaga situations, despite typically underestimating the amplitude of the harbour oscillation. The method described in this paper could be implemented in congestion with the neural network method of Vich and Romero (2021) to get improved forecasts. A working system using atmospheric and oceanographic models to predict meteotsunamis was tested for the Adraitic Sea (Denamiel et al., 2019), as well as for the Balearic Islands (Mourre et al., 2021). These models could benefit from the method explained in this paper at the first step, with a possibility of assessing the similarity of each upcoming day to extracted clusters. After that, only synoptics that get high SSIM scores can be used to force the higher-resolution atmospheric and ocean models.

https://doi.org/10.5194/egusphere-2024-1601
Preprint. Discussion started: 5 June 2024

Finally, the k-medoids SSIM method could be used on its own. The main problem of predicting extreme HF oscillations, and in particular meteotsunamis is that small changes in speed or direction of the pressure disturbance can result in great differences in the HF heights at observational locations as pointed out by Mourre et al. (2021). There is a potential for overcoming this by applying the method put forward in this paper by considering the larger domain of the Adriatic Sea (as presented in Fig. 1) and an additional smaller domain center around the observed harbour. Linking the SSIM score of the larger and smaller domain to the values of HF heights there could be a possibility of direct forecast that could be, in principle, fast and reliant. Although there is still work to be done to confirm or deny the feasibility of a warning system reliant on the k-medoid SSIM method, the current result of SSIM scores, as presented in Fig. 10, show that there is a possibility of this system being functional since all days with HF extremes score high (above average) SSIM scores.

Author contribution

All of the authors helped with the conceptualization of the paper. KR did the data analysis, JS and KR wrote the manuscript while KR, JS and MV edited and corrected the text. JS supervised the analysis and the writing of the manuscript.

Competing interests

The authors declare that they have no conflict of interest.

Acknowledgements

ERC StG 853045 SHExtreme, HRZZ IP-2019-04-5875 StVar-Adri. Iva Međugorac and Mirko Orlić (both Department of Geophysics, Faculty of Science, University of Zagreb), Srđan Čupić and Marko Mlinar (Hydrographic Institute of Republic of Croatia) for diligently taking care of tide gauge stations Rovinj, Bakar, Zadar, Split, Ploče and Dubrovnik, and ensuring high quality data. Hrvoje Kalinić, Leon Ćatipović (Faculty of Science, University of Split) and Frano Matić (University of Split) for fruitful discussions related to selection of classification algorithm.

https://doi.org/10.5194/egusphere-2024-1601
Preprint. Discussion started: 5 June 2024

References

Bechle, A. and Wu, C.: The Lake Michigan meteotsunamis of 1954 revisited. Natural Hazards, 74, 155-177, https://doi.org/10.1007/s11069-014-1193-5, 2014.

Bechle, A.J., Wu, C.H., Kristovich, D.A.R., Anderson, E.J., Schwab, D.J., and Rabinovich, A.B.: Meteotsunamis in the Laurentian Great Lakes. Sci Rep 6, 37832, https://doi.org/10.1038/srep37832, 2016.

Belušić, D., Grisogono, B., and Klaić, Z.B.: Atmospheric origin of the devastating coupled air-sea event in the east Adriatic. Journal of Geophysical Research, 112 (D17). https://doi.org/10.1029/2006JD008204, 2007.

Copernicus Climate Change Service (C3S): ERA5: Fifth generation of ECMWF atmospheric reanalyses of the global climate. Copernicus Climate Change Service Climate Data Store (CDS), https://cds.climate.copernicus.eu/cdsapp#!/home, 2017. Last accessed on 23 January 2024.

Denamiel, C., Šepić, J., Ivanković, D., and Vilibić, I.: The Adriatic Sea and Coast modelling suite: Evaluation of the meteotsunami forecast component, Ocean Modelling, 135, 71-93,1463-5003, https://doi.org/10.1016/j.ocemod.2019.02.003, 2019 .

Di Bernardino, A., Iannarelli, A.M., Casadio, S., Pisacane, G., Mevi, G., and Cacciani, M.: Classification of synoptic and local-scale wind patterns using k-means clustering in a Tyrrhenian coastal area (Italy). Meteorol Atmos Phys 134, 30, https://doi.org/10.1007/s00703-022-00871-z, 2022.

Dusek, G., DiVeglio, C., Licate, L., Heilman, L., Kirk, K., Paternostro, C., and Miller, A.: A meteotsunami climatology along the U.S. East Coast. Bull. Am. Meteorol. Soc., 100, 1329-1345, https://doi.org/10.1175/BAMS-D-18-0206.1, 2019.

Elken, J., Zujev, M., She, J., and Lagemaa, P.: Reconstruction of Large-Scale Sea Surface Temperature and Salinity Fields Using Sub-Regional EOF Patterns From Models. Frontiers in Earth Science, 7, 296-6463, https://www.frontiersin.org/articles/10.3389/feart.2019.00232, 2019.

Ewing, M., Press, F., and Donn, W.J.: An explanation of the Lake Michigan wave of 26 June 1954. Science 120:684–686. https://doi.org/10.1126/science.120.3122.684, 1954.

Ferrarin, C., Bajo, M., Benetazzo, A., Cavaleri, L., Chiggiato, J., Davison, S., Davolio, S., Lionello, P., Orlić, M., and Umgiesser, G.: Local and large-scale controls of the exceptional Venice floods of November 2019. Prog Oceanogr 197:102628. https://doi.org/10.1016/j.pocean.2021.102628, 2021.

Fine, I.V., Rabinovich, A.B., Thomson, R.E., and Kulikov, E.A.: Numerical Modeling of Tsunami Generation by Submarine and Subaerial Landslides, in: Submarine Landslides and Tsunamis, edited by Yalçiner, A.C., Pelinovsky, E.N., Okal, E., Synolakis, C.E. NATO Science Series, vol 21. Springer, Dordrecht, 69–88, https://doi.org/10.1007/978-94-010-0205-9_9, 2003.

Fontseré, E.: Les 'seixes' de la costa catalana. Servei Meteorologic de Catalunya, Notes d'Estudi, (in Catalan), 1934.

Grisogono, B. and Belušić, D.: A review of recent advances in understanding the meso- and microscale properties of the severe Bora wind. Tellus A, 61(1), 1–16. https://doi.org/10.1111/j.1600-0870.2008.00369.x, 2009.

https://doi.org/10.5194/egusphere-2024-1601
Preprint. Discussion started: 5 June 2024

Haigh, I.D., Marcos, M., Talke, S.A., Woodworth, P.L., Hunter, J.R., Hague, B.S., Arns, A., Bradshaw, E., and Thompson, P.: GESLA Version 3: a major update to the global higher-frequency sea-level dataset. Geosci. Data J., 10, 293–314, https://doi.org/10.1002/gdj3.174, 2022.

Hartigan, J.A. and Wong, M.A.: Algorithm AS 136: A K-Means Clustering Algorithm. Journal of the Royal Statistical Society. Series C (Applied Statistics) 28, 1, 100–108. https://doi.org/10.2307/2346830, 1979.

Heidarzadeh, M., and Rabinovich, A.B.: Combined hazard of typhoon-generated meteorological tsunamis and storm surges along the coast of Japan. Nat Hazards 106:1639–1672, https://doi.org/10.1007/s11069-020-04448-0, 2021.

Hibiya, T. and Kajiura, K.: Origin of the Abiki phenomenon (a kind of seiche) in Nagasaki Bay. Journal of the Oceanographical Society of Japan, 38, 172–182. https://doi.org/10.1007/BF02110288, 1982.

Hodžić, M.: Long gravity waves on the sea surface caused by cyclones and free oscillations (seiches) in the Vela Luka Bay on the Adriatic. Rivista di Meteorologia Aeronautica, 48 (1-2), 47-52, 1988.

Hoffmann, P., Lehmann, J., Fallah, B., and Hattermann, F.F.: Atmosphere similarity patterns in boreal summer show an increase of persistent weather conditions connected to hydro-climatic risks. Sci Rep 11, 22893, https://doi.org/10.1038/s41598-021-01808-z, 2021.

Honda, K., Terada, T., Yoshida, Y., and Isitani, D.: Secondary undulations of oceanic tides. Journal of the College of Science (Imperial University, Tokyo, Japan), 24, 1-113, 1908.

Jansà, A. and Ramis. C.: The Balearic rissaga: from pioneering research to present-day knowledge. Nat. Hazards, 106, 1269-1297, https://doi.org/10.1007/s11069-020-04221-3, 2021.

Jansà, A., Monserrat, S., and Gomis, D.: The rissaga of 15 June 2006 in Ciutadella (Menorca), a meteorological tsunami. Adv. Geosci., 12, 1–4, https://doi.org/10.5194/adgeo-12-1-2007, 2007.

Kaufmann, L. and Rousseeuw, P.: Clustering by Means of Medoids. Data Analysis based on the L1-Norm and Related Methods. 405-416, 1987.

Kodinariya, T.M. and Makwana, P.R.: Review on determining number of Cluster in KMeans Clustering. Int J Adv Res Comput Sci Manag Stud 1(6):90–95, https://api.semanticscholar.org/CorpusID:10090179, 2013.

Kohonen, T.: Self-Organization and Associative Memory. Springer Berlin, Heidelberg, 3rd edition, 312 pp., ISBN 978-3-540-51387-2, https://doi.org/10.1007/978-3-642-88163-3, 1989.

Levin, B. and Nosov, M.: Physics of Tsunamis, Springer, Dordrecht, 327 pp. 2009.

Lewis, C., Smyth, T., Williams, D., Neumann, J., and Cloke, H.: Meteotsunami in the United Kingdom: the hidden hazard. Nat. Hazards Earth Syst. Sci., 23, 2531–2546, https://doi.org/10.5194/nhess-23-2531-2023, 2023.

Lionello, P., Cavaleri, L., Nissen, K.M., Pino, C., Raicich, F. and Ulbrich, U.: Severe marine storms in the Northern Adriatic: characteristics and trends. Phys Chem Earth Parts a/b/c 40–41:93–105. https://doi.org/10.1016/j.pce.2010.10.002, 2012.

Lorenz, E.N.: Empirical orthogonal functions and statistical weather prediction. Sci. Rep. No. 1, Statistical Forecasting Project, M.I.T., Cambridge, MA, 48 pp, 1956.

https://doi.org/10.5194/egusphere-2024-1601
Preprint. Discussion started: 5 June 2024

Medvedev, I.P., Rabinovich, A.B., and Šepić, J.: Destructive coastal sea level oscillations generated by Typhoon Maysak in the Sea of Japan in September 2020. Sci Rep 12, 8463, https://doi.org/10.1038/s41598-022-12189-2, 2022.

Milligan, G.W. and Cooper, M.C.: A study of standardization of variables in cluster analysis. Journal of Classification, 5(2), 181–204, https://doi.org/10.1007/bf01897163, 1988.

Monserrat, S. and Thorpe, A.J.: Use of ducting theory in an observed case of gravity waves. J. Atmos. Sci., 53, 1724–1736, https://doi.org/10.1175/1520-0469(1996)053<1724:UODTIA>2.0.CO;2, 1996.

Monserrat, S., Vilibić, I., and Rabinovich, A.B.: Meteotsunamis: atmospherically induced destructive ocean waves in the tsunami frequency band. Nat. Hazards Earth Syst. Sci., 6, 1035–1051, https://doi.org/10.5194/nhess-6-1035-2006, 2006.

Mourre, B., Santana, A., Buils, A., Gautreau, L., Ličer, M., Jansà, A., Casas, B., Amengual, B., and Tintoré, J.: On the potential of ensemble forecasting for the prediction of meteotsunamis in the Balearic Islands: sensitivity to atmospheric model parameterizations. Nat Hazards 106, 1315–1336, https://doi.org/10.1007/s11069-020-03908-x, 2021.

Navarra, A. and Simoncini, V.: Empirical Orthogonal Functions, in: A Guide to Empirical Orthogonal Functions for Climate Data Analysis, Springer Dordrecht, 39-67, https://doi.org/10.1007/978-90-481-3702-2, 2010.

Orlić, M.: About a possible occurrence of the Proudman resonance in the Adriatic. Thalassia Jugoslavica, 16, 78-88, 1980.

Orlić, M.: The first attempt at cataloguing tsunami-like waves of meteorological orign in Croatian coastal waters. Acta Adriatica, 56(1), 83-96, 2015.

Pandžić, K. and Likso, T.: Eastern Adriatic typical wind field patterns and large-scale atmospheric conditions. Int. J. Climatol., 25: 81-98. https://doi.org/10.1002/joc.1085, 2005.

Pellikka, H., Šepić, J., Lehtonen, I., and Vilibić, I.: Meteotsunamis in the northern Baltic Sea and their relationship to atmospheric synoptic patterns. Weather and Climate Extremes, 38, 100527, https://doi.org/10.1016/j.wace.2022.100527, 2022.

Pérez-Gómez, B., García-León, M., García-Valdecasas, J., Clementi, E., Mösso Aranda, C., Pérez-Rubio, S., Masina, S., Coppini, G., Molina-Sánchez, R., Muñoz-Cubillo, A., García Fletcher, A., Sánchez González, J.F., Sánchez-Arcilla, A., and Álvarez Fanjul, E.: Understanding sea level processes during western Mediterranean storm Gloria. Front Mar Sci 8:647437, https://doi.org/10.3389/fmars.2021.647437, 2021.

Proudman, J.: The effects on the sea of changes in atmospheric pressure. Geophysical Supplement to Monthly Notices of the Royal Astronomical Society, 2 (4), 197–209, 1929.

Pugh, D. and Woodworth, P.: Sea-level science: understanding tides, surges, tsunamis and mean sea-level changes. Cambridge University Press, 395 pp., ISBN 9781107028197, 2014.

Pupić Vurilj, M., Brnas, T., Ruić, K., Šepić, J. and Balić, M.: Mediterranean meteotsunamis of May 2021 and June 2022: Observations, data analysis and synoptic background. Geofizika, 40 (2), 179-205. https://doi.org/10.15233/gfz.2023.40.8, 2023.

Rabinovich, A.B.: Seiches and Harbor Oscillations, in: Handbook of Coastal and Ocean Engineering. World Scientific, 193-236. https://doi.org/10.1142/9789812819307_0009, 2009.

https://doi.org/10.5194/egusphere-2024-1601
Preprint. Discussion started: 5 June 2024

Rabinovich, A.B.: Twenty-seven years of progress in the science of meteorological tsunamis following the 1992 Daytona Beach event. Pure Appl. Geophys., 177, 1193-1230, https://doi.org/10.1007/s00024-019-02349-3, 2020.

Rabinovich, A.B. and Monserrat, S. Meteorological tsunamis near the Balearic and Kuril Islands: Descriptive and statistical analysis. Nat Hazards 13, 55–90, https://doi.org/10.1007/BF00156506, 1996.

Rabinovich, A.B., Šepić, J., and Thomson, R.: Strength in numbers: the tail end of Typhoon Songda combines with local cyclones to generate extreme sea level oscillation on the British Columbia and Washington coasts during mid-October 2016. Journal of Physical Oceanography, 131-155, https://doi.org/10.1175/JPO-D-22-0096.1, 2023.

Raicich, F.: On the contributions of atmospheric pressure and wind to daily sea level in the northern Adriatic Sea. Cont. Shelf Res. 30, 1575–1581, https://doi.org/10.1016/j.csr.2010.05.017, 2010.

Ramis, C. and Jansà, A.: Condiciones meteorológicas simultáneas a la aparición de oscilaciones del nivel del mar de amplitud extraordinaria en el Mediterráneo Occidental. Rev. Geofisc., 39, 35-42, 1983.

Roundy, P.E.: On the Interpretation of EOF Analysis of ENSO, Atmospheric Kelvin Waves, and the MJO. J. Climate, 28, 1148–1165, https://doi.org/10.1175/JCLI-D-14-00398.1, 2015.

Reusch, D.B., Alley, R.B., and Hewitson, B.C.: North Atlantic climate variability from a self-organizing map perspective. Journal of Geophysical Research, 112(D2). https://doi.org/10.1029/2006jd007460, 2007.

Rousseeuw J.P.: Silhouettes: a graphical aid to the interpretation and validation of cluster analysis. Journal of Computational and Applied Mathematics 20, 53- 65, 1987.

Ruić, K., Šepić, J., Mlinar, M., and Međugorac, I.: Contribution of high-frequency (T < 2 h) sea level oscillations to the Adriatic sea level maxima. Natural Hazards, 116, 3747-3777, https://doi.org/10.1007/s11069-023-05834-0, 2023.

Suursaar, Ü., Kullas, T., Otsmann, M., Saaremäe, I., Kuik, J., and Merilain, M.: Cyclone Gudrun in January 2005 and modelling its hydrodynamic consequences in the Estonian coastal waters. Boreal Env Res 11:143–159, 2006.

Šepić, J. and Orlić, M.: Adriatic meteotsunami catalogue, https://projekti.pmfst.unist.hr/floods/meteotsunamis/. Accessed: 21 April 2024, 2024.

Šepić, J., Vilibić, I., and Monserrat S.: Teleconnections between the Adriatic and the Balearic meteotsunamis. Phys. Chem. Earth, 34, 928-937, https://doi.org/10.1016/j.pce.2009.08.007, 2009.

Šepić J., Vilibić, I., Lafon, A., Macheboeuf, L., and Ivanović, Z.: High-frequency sea level oscillations in the Mediterranean and their connection to synoptic patterns. Progress in Oceanography, 137, 284-298, https://doi.org/10.1016/j.pocean.2015.07.005, 2015a.

Šepić J., Vilibić, I., Rabinovich, A.B., and Monserrat, S.: Widespread tsunami-like waves of 23-27 June in the Mediterranean and Black Seas generated by high-altitude atmospheric forcing. Scientific Reports, 5, 11682, https://doi.org/10.1038/srep11682, 2015b.

Šepić J., Vilbić, I., and Fine, I.: Northern Adriatic meteorological tsunamis: assessment of their potential through ocean modeling experiments. Journal of Geophysical Research, 120, 2993-3010, https://doi.org/10.1002/2015JC010795, 2015c.

https://doi.org/10.5194/egusphere-2024-1601
Preprint. Discussion started: 5 June 2024

Šepić, J., Vilibić, I., and Monserrat, S.: Quantifying the probability of meteotsunami occurrence from synoptic atmospheric patterns. Geophys. Res. Lett., 43, 10377-10384, https://doi.org/10.1002/2016GL070754, 2016.

Thomson, R. E. and Emery, W. J.: Data analysis methods in physical oceanography. Elsevier, Amsterdam, 2014.

Ursell F.: Edge waves on a sloping beach. Proc. R. Soc. Lond. A21479–97, http://doi.org/10.1098/rspa.1952.0152, 1952.

Vich, MdM. and Romero, R.: Forecasting meteotsunamis with neural networks: the case of Ciutadella harbour (Balearic Islands). Nat Hazards 106, 1299–1314, https://doi.org/10.1007/s11069-020-04041-5, 2021.

Vilibić, I. and Šepić, J.: Destructive meteotsunamis along the eastern Adriatic coast: overview. Physics and Chemistry of the Earth, 34, 904-917, https://doi.org/10.1016/j.pce.2009.08.004, 2009.

Vilibić, I. and Šepić J.: Global mapping of nonseismic sea level oscillations at tsunami timescales. Scientific Reports, 7, 40818, https://doi.org/10.1038/srep40818, 2017.

Wilson, B.: Seiches. Advances in Hydrosciences, 8, 1-94, https://doi.org/10.1016/B978-0-12-021808-0.50006-1, 1972.

Zemunik, P., Vilibić, I., Šepić, J., Pellikka, H., and Ćatipović, L.: MISELA: 1-minute sea-level analysis global dataset. Earth Syst. Sci. Data, 13, 4121-4132, https://doi.org/10.5194/essd-2021-134, 2021a.

Zemunik, P., Vilibić, I., Šepić, J., Pellikka, H., and Ćatipović, L.: MISELA: Minute Sea-Level Analysis, Marine Data Archive [data set], https://doi.org/10.14284/456, 2021b.

Zemunik, P., Denamiel, C., Šepić, J., and Vilibić, I.: High-frequency sea-level analysis: global distributions. Global Planet. Change, 210, 103775, https://doi.org/10.1016/j.gloplacha.2022.103775, 2022a.

Zemunik, P., Denamiel, C., Williams, J., and Vilibić, I.: High-frequency sea-level extremes: Global correlations to synoptic atmospheric patterns. Weather and Climate Extremes, 38, 100516, https://doi.org/10.1016/j.wace.2022.100516, 2022b.

Wang, Z. and Bovik, A.C.: Mean squared error: Love it or leave it? A new look at Signal Fidelity Measures, IEEE Signal Processing Magazine, 26, 98-117, https://doi.org/10.1109/msp.2008.930649, 2009.

Wang, Z., Bovik, A.C., Sheikh, H.R., and Simoncelli, E.P.: Image quality assessment: from error visibility to structural similarity, IEEE Trans Image Process, 13, 600-612, https://doi.org/10.1109/tip.2003.819861, 2004.

Winderlich, K., Dalelane, C., and Walter, A.: Classification of synoptic circulation patterns with a two-stage clustering algorithm using the modified structural similarity index metric (SSIM), Earth Syst. Dynam. Discuss. [preprint], https://doi.org/10.5194/esd-2023-34, in review, 2023.